UNITED STATES DEPARTMENT OF THE INTERIOR
GEOLOGICAL SURVEY

THE MECHANISM OF PERMEABILITY REDUCTION DURING FLOW OF HYDROTHERMAL FLUIDS THROUGH WESTERLY GRANITE

P.J. Vaughan, D.E. Moore, C.A. Morrow, and J.D. Byerlee

Open-File Report
85-262

INTRODUCTION

The permeability of intact and fractured Westerly Granite has been measured under conditions in which the fluid was passed through the rock down an applied temperature gradient (Morrow et al., 1981; Moore et al., 1983). These experiments simulated the movement of fluids around encapsulated radioactive waste deposited in mined cavities. Substantial reductions in permeability occurred during these experiments. As an example, permeability decreased by a factor of 25 during experiment NWD 2200, which lasted for 2 weeks (labelled W300 in Moore et al., 1983). The aim of this paper is to provide some insight into the physical characteristics of the rock which are responsible both for its permeability and for the changes in permeability with time during the experiments.

The permeability of Westerly Granite is strongly influenced by the effective pressure, defined as confining pressure minus pore pressure. Increasing the effective pressure by a factor of 10 causes the permeability of Westerly Granite to decrease by a factor of 10 (Brace et al., 1968). This decrease was attributed to the closure of low aspect ratio cracks. Aspect ratio is defined as the ratio of the shortest to the longest dimension of a crack.

Further studies (Brace, 1977; Hadley, 1976) have demonstrated conclusively that low aspect ratio cracks control the permeability of Westerly Granite. Resistivity measurements made on Westerly Granite had indicated that the hydraulic radius was relatively independent of pressure (Brace et al., 1968), even though one would expect the hydraulic radius to change with effective pressure due to probable changes in the mean aspect ratio of cracks. However, Brace (1977) showed that the distribution of crack dimensions (Hadley, 1976) is such that, as effective pressure is raised, the continued closing of the lowest aspect ratio cracks does not significantly change the mean aspect ratio of the remaining open cracks. In Westerly Granite the high aspect ratio cracks (pores) are isolated and do not form continuous fluid pathways (Montgomery and Brace, 1975). Thus, in looking for an explanation of the large permeability reduction observed by Moore et al. (1983) it seems most worthwhile to examine the low aspect ratio cracks. It is believed that most low aspect ratio cracks in granitic rocks are closed at an effective pressure somewhere in the range of 50 MPa (Simmons and Caruso, 1983) to 100-200 MPa (Warren, 1977). Because the effective pressure in the experiment of Moore et al. (1983) was 40 MPa, some fraction of the original set of low aspect ratio cracks should have remained open.

The reductions in permeability observed during the experiments of Moore et al. (1983) were attributed to filling of cracks which comprised the fluid pathways by material that had been dissolved in other regions of the sample where the temperature was higher (Morrow et al., 1981; Moore et al., 1983). Based on SEM (scanning electron microscope) observations they identified silica and zeolitic fibers lining fracture surfaces in a sample that had been fractured prior to testing. Morrow et al. (1981) concluded that the deposition of these materials was the probable cause of the permeability reduction.

The discharged fluids were periodically collected during the permeability experiments and chemically analyzed (Moore et al., 1983). Thermodynamic calculations indicated that, for most experiments, these fluids were supersaturated with respect to quartz for the temperatures measured at the outer surface of the cylindrical samples. Thus precipitation of quartz could occur at least near the outer edge of the sample; however, this would not rule out the possibility of precipitation of some other silicate instead. In fact, precipitation of zeolites on feldspars has been observed (Morrow et al., 1981). The transport and precipitation of material in cracks over grain-scale and larger distances are termed crack-sealing processes (Smith and Evans, 1984).

A different potential mechanism for permeability reduction is crack healing, as opposed to crack sealing. Crack healing occurs by dissolution and reprecipitation of minerals on a local scale within cracks such that the precipitated material is in crystallographic continuity with the surrounding grain (Smith and Evans, 1984; Simmons and Richter, 1976). Smith and Evans (1984) conducted annealing experiments on a fractured pure quartz sample to study crack healing under hydrothermal conditions. Their results emphasized the importance of a pore fluid to the crack healing process, because crack healing occurred at 400°C in the presence of a pore fluid but it did not occur at 600°C in the absence of such a fluid.

In experiments with $P_{fluid}=P_{total}$ at 200°C (Smith and Evans, 1984), crack healing did not occur for experiment lengths of up to 2 days. The original surface structure of cracks, including surface steps and hackle marks, was still present. The crack healing results, therefore, indicate that there is a significant temperature dependence. These observations suggest that, for temperatures lower than 200°C, crack healing would not be significant for times on the order of the experimental length. Thus, we would expect crack healing to be significant only for those portions of our samples that were above 200°C during the experiments.

Although a reduction of permeability in intact granite has been found in several experiments (Morrow et al., 1981; Moore et al.,1983), detailed observations of the cracks in intact samples using the SEM were not made. One goal of this work was to examine the low aspect ratio cracks, in order to determine what changes might have occurred during the experiments. Such observations could provide information regarding the mechanism of permeability reduction. For example, SEM studies of cracks in different parts of the sample might reveal where crack-sealing or crack-healing processes had occurred. Furthermore, the composition of material contained in the low aspect ratio cracks may be determined, in a qualitative sense, by energy dispersive x-ray analysis (EDAX).

To accomplish this goal, we examined one of the intact Westerly Granite samples (NWD 2200, called W300 in Moore et al., 1983) utilizing an optical microscope and a scanning electron microscope (SEM). Westerly Granite was chosen because information is readily available on this rock, including the statistical distribution of crack dimensions (Sprunt and Brace, 1974; Hadley, 1976). This particular sample was chosen because the permeability reduction observed was representative of that found in the intact granite samples.

A second goal of this study was to determine the effect of introducing an artificial fluid pathway in the rock, in this case, a polished interface. The polished interface provided an opportunity to examine a flat surface along which flow had occurred. This surface could potentially show dissolution and/or precipitation of material and thereby give some indication of where in the samples these processes might have occurred. The results of this experiment differed from expectations and, as a result, bear no specific relationship to the central question regarding the mechanism of the permeability reduction in intact samples. Thus, the discussion of this experiment is given in Appendix B.

PERMEABILITY EXPERIMENTS

Procedures

The intact sample of Westerly Granite used in experiment NWD 2200 had a 7.62 cm outside diameter, a 1.27 cm borehole diameter and length of 8.89 cm (Figure 1). The experiments consisted of passing a fluid down a small pore pressure gradient that was maintained between the axial internal borehole and the outer edge of a cylindrical rock sample. The fluid was initially deionized water. The fluid in the borehole was heated by a gold-coated resistance heater (Figure 1). Further details on the NWD 2200 experiment are given in Moore et al. (1983).

The procedure for determination of permeabilities in samples subjected to a temperature gradient is detailed in several publications (Morrow et al., 1981; Moore et al., 1983). Briefly, the flow rates are determined by measuring the volume of water pumped into the borehole during an experiment. Permeabilities are calculated from the flow rates and the pore pressure gradient using Darcy's Law. Permeability data for the NWD 2200 experiment are listed in Table 1 and the chemical data in Table 2. Permeability and chemical data are also listed for a second experiment, NWD 3300, in these tables. The NWD 3300 experiment is discussed in Appendix B. Permeability is plotted against time from the initial heating for both experiments (Figure 2). The data for NWD 2200 have been published elsewhere (Moore et al., 1983) but those for NWD 3300 are presented here for the first time.

SCANNING ELECTRON MICROSCOPY

Procedures

The samples from each experiment were examined in a Cambridge Stereoscan 250* scanning electron microscope (SEM) equipped with a Tracor Northern* energy dispersive x-ray detector. This detector proved very useful for making qualitative determinations of the composition of filling in cracks and for identifying the minerals in the SEM.

---

* Use of commercial trade names is for descriptive purposes only and does not imply endorsement by the U.S. Geological Survey.

A cylindrical butt of the starting material and two butts of the NWD 2200 sample were highly polished with a series of alumina powders down to 1 micron. The butts from NWD 2200 were taken from cores cut parallel to the axis of the sample. The polished surfaces of these butts were located about 2 cm from one end of the sample. The butts were polished with a series of alumina powders with grit sizes down to 1 micron and finally with 0.3 micron Ce_2O_3. The surface preparation consisted of ion beam thinning which removes the damaged layers from the surface produced by the grinding and polishing procedure (Sprunt and Brace, 1974). A Technics model MIM 4* was used with high voltage set at 6 kV and a beam current of about 1 mA. For further details on the thinning procedure see Sprunt and Brace (1974). Topography introduced by long thinning times can obscure the original features of a sample. Sprunt and Brace(1974) found that significant topography developed for thinning times greater than 6 hours. Thus we used thinning times of 5 hours.

In addition to these samples, two crack sections (Simmons and Richter, 1976) were prepared from NWD 2200 for both optical and SEM examination. Crack sections are about 150 microns thick as compared to standard thin sections, which are only 30 microns thick. These sections were oriented the same as the butts, normal to the axis of the sample, but they were located near the middle of the sample cylinder. The greater thickness of the crack sections serves two purposes. First, the cracks can be examined in the third dimension by adjusting the focus on a petrographic microscope and, second, the thicker sample is less likely to have cracks introduced by the thin-sectioning process. The crack sections were highly polished on both sides, using a range of diamond pastes from 6 to 1 micron and a final polish with 0.3 micron alumina. The polished surface provided satisfactory SEM images, with the crack fillings showing only minor disturbance by the polishing. These crack sections were not ion-milled.

Detailed SEM observations were made on the prepared butt of the Westerly starting material and on two butts from sample NWD 2200. Three areas were examined on the two butts from the NWD 2200 experimental sample. They were located approximately 1 mm from the outer edge, 1 mm from the central borehole and 5 mm from the central borehole (Figure 3). The areas immediately adjacent to the borehole and the outer edge were chosen because they represent the two extremes with regard to temperature in the samples. The area located 5 mm from the borehole was chosen because kinetic calculations indicate that in this region of the sample precipitation of quartz will be greatest. These calculations are discussed in detail in Appendix A. A mosaic of overlapping SEM micrographs covering an area of 5 mm^2 (100X, about 20 grains) was constructed for each of the three locations in the NWD 2200 sample. Mosaics are a useful way to map the cracks in an area consisting of several grains because they provide a better statistical sample than may be obtained from isolated micrographs. Specific locations along intragranular cracks and grain boundaries were chosen on these mosaics for examination at much higher magnification. An attempt was made to choose areas that were as representative as possible for the mosaics given the constraints of the relatively coarse grain size and the many different types of grain boundaries present among the various minerals.

The SEM could also be operated in a mode in which an image was formed by collecting electrons emitted from the sample at high angles to the surface. This mode, called back-scattered electron imaging (BSE) is sensitive to the mean atomic number in an area, making it possible to identify minerals based on differences in the intensity of the back-scattered radiation. In addition to the SEM mosaic, a similar mosaic of BSE micrographs was constructed for each of the areas chosen. Both grain boundary cracks and intragrain cracks were more readily identifiable in the BSE mode at relatively low magnifications (less than 500X). Cracks of less than 0.1 microns width do not contribute significantly to permeability based on the distribution of crack widths (Brace, 1977). Therefore, we have examined those larger cracks which are easily visible in the SEM at 100X. We utilize the terminology presented by Simmons and Richter (1976) regarding cracks.

OBSERVATIONS

Starting Material

A virgin sample of Westerly Granite was examined in order to help distinguish between features that were initially present in the rock and those that were formed as a result of the experiment. These observations also permitted a qualitative comparison of the starting material with Westerly Granite samples studied by Sprunt and Brace (1974) and Hadley (1976). Crack characteristics of the starting material are generally consistent with the observations of Sprunt and Brace (1974) and Hadley (1976), on virgin Westerly Granite except for some transgranular cracks that were present in our sample. Transgranular cracks are those intragrain cracks which meet two grain boundaries. Such cracks are present in some of the smaller grains, especially quartz, and have maximum length of about 300 microns in the 5 mm^2 area examined.

Most intragranular cracks are open, that is, they do not contain a filling material. However, these cracks are sometimes filled along short portions of their length, in which case the filling material is referred to as a bridge. Crack bridges were first observed by Sprunt and Brace (1974) in Westerly Granite. In the starting material the bridges are composed primarily of a silica-rich material.

The grain boundaries between the two feldspars are almost always uncracked. However, about 50% of grain boundaries between quartz grains and between quartz and feldspar are cracked. Figure 4a contains an example of a quartz - K-feldspar grain boundary that is not cracked, whereas 4b shows an intragranular crack in quartz intersecting a cracked quartz-K-feldspar grain boundary. The grain boundary cracks are about the same length as the diameter of quartz grains.

Pores are present in all three of the major phases. They are most abundant in plagioclase, less abundant in K-feldspar and least common in quartz. The pores present in plagioclase occur preferentially in distinct compositional zones. In places where intragrain cracks run through the zones of high pore density the crack surfaces are rough, but, generally, the intragrain crack surfaces are smooth.

NWD 2200

As a general characteristic, the crack density in the experimental sample, NWD 2200, was greater in the area near the outer edge of the cylinder than in the two areas close to the borehole. Fillings occur in many of the cracks in all three areas. However, there are some important differences in the texture and local distribution of the fillings in the three areas.

Crack dimensions are of fundamental importance in determining the crack porosity of a rock and, thereby, the permeability. The arithmetic mean of crack widths near the borehole, near the outer edge and in the starting material are, 0.3, 0.4 and 0.4 microns, respectively. Therefore, no significant variation in crack width occurs among these samples. In addition to intragrain cracks and grain boundary cracks there are also intergrain cracks which pass through grain boundaries and may pass from one mineral into another.

Intragrain Cracks - NWD 2200

With regard to the type and distribution of intragrain cracks, the quartz in the NWD 2200 sample is markedly different from the two feldspars. For this reason, the descriptions of cracks in quartz and those in the feldspars are separated.

Quartz

In sample NWD 2200, all three of the major minerals contain intragrain cracks, with the highest density occurring in quartz. Several large intersecting cracks form a loose network which connects the grain boundaries in most quartz grains. These cracks are easily distinguishable in both the petrographic microscope and 100X SEM micrographs, making it possible to correlate optical and SEM observations. As quartz grains tend to occur in clusters, the intragrain cracks are intimately associated with grain boundary cracks and, in the SEM, it is difficult to distinguish large intragrain cracks from cracked grain boundaries (Figure 5). However, it was possible to make this distinction by examining the same areas in crack sections in a petrographic microscope. Intragrain cracks have been identified and marked in Figure 5 with small arrows. The unmarked cracks in Figure 5 are grain boundary cracks.

The length of intragrain cracks ranges from the diameter of a pore (a few microns) up to the grain size (several hundred microns, Figure 5). The outer edge of the NWD 2200 sample has a higher density of transgranular cracks than does the starting material. However, the density of transgranular cracks in the two areas of the NWD 2200 sample near the borehole appears to be lower than in the starting material. The intragrain cracks in the starting material (Figure 6a) are similar in size and appearance to those in the two areas near the borehole (Figures 6c and 6d). The width of the large intragrain cracks in the starting material and in all three areas of the NWD 2200 sample ranges from 0.1 to 1.0 microns, disregarding the presence of filling (Figure 6). The walls of the larger cracks in NWD 2200 have a high degree of surface roughness,

making it difficult to estimate their width accurately (Figure 6b). In isolated places the intragrain cracks are highly curved but generally they are straighter than grain boundary cracks.

In addition to large intragrain cracks, many smaller ones occur which are not observable at a magnification of 100X. For example, Figure 7 shows a quartz grain near the outer edge of the NWD 2200 sample containing a narrow intragrain crack which could only be distinguished at lower magnifications as a chain of pores. This particular microcrack is less than 0.1 micron wide and may even be completely closed. A gradation exists between the rough surfaces of large cracks as in Figure 6b and the clearly separated pores of Figure 7.

Feldspar

Large intragrain cracks in the feldspars are generally similar to those in quartz, although they are somewhat less numerous and have widths of as much as a few microns (Figure 8a). The intragrain cracks in feldspar in the starting material have a high surface roughness that is related to the high density of pores in plagioclase. In places where the intragrain cracks intersect pores the crack surface is scalloped (Figure 8b). Pore density in K-feldspar is lower than in plagioclase and, correspondingly, there is less crack surface roughness. Otherwise, intragrain cracks in the two feldspars are similar. High surface roughness appears to be enhanced as a result of the experiment because pores occur more frequently along intragranular cracks in the experimental sample (Figure 8b) than in the starting material (Figure 8a). In this regard, the behavior of the feldspars is similar to that of quartz. The feldspars also contain both open and filled cracks in all three areas (Figures 8c, 8d, 9b).

The grain size of the feldspars is larger than that of quartz, but the maximum crack length is about the same (300 microns). Thus, the feldspars contain fewer transgranular cracks. The intragranular cracks in feldspars can be several microns wide in places because of the high surface roughness. Cleavage cracks occur in the feldspars, but such cracks are usually restricted to the interiors of grains and are narrower than the other intragrain cracks (Figure 10, marked C). The cleavage cracks also are distinguishable by their orientation and lack of curvature.

Grain Boundary Cracks

Simmons and Richter (1976) classified grain boundary cracks as coincident, that is, following the grain boundary; or non-coincident, occurring within a single grain and intersecting a grain boundary. The experimental sample contains arrays of intersecting, transgranular cracks which form networks by meeting cracked grain boundaries (Figure 4b). Such transgranular cracks are especially prevalent in quartz. Because these intragranular cracks meet grain boundaries they might be classified as non-coincident grain boundary cracks. However, the question of whether these cracks are specifically related to the grain boundary is difficult to answer. In discussing grain boundary cracks, we refer only to the coincident grain boundary cracks.

Most of the grain boundaries between feldspars in the starting material were closed, and they have remained closed during the experiment in all three areas examined (Figure 9). Out of 10 locations examined along different plagioclase - K-feldspar grain boundaries in the NWD 2200 sample, only one grain boundary appeared cracked. The grain boundaries between quartz and the feldspars and those between quartz and the minor minerals in the NWD 2200 sample are frequently cracked. However, the data are insufficient to determine whether a significant difference exists between the NWD 2200 sample and the starting material in this regard. The grain boundaries between quartz grains were often cracked in the NWD 2200 sample and the interconnection of these cracks with intragranular cracks forms a network that is generally not present in feldspar.

Pores

Pores are present in all three of the major phases. The pores are most abundant in plagioclase, less abundant in K-feldspar, and least common in quartz. They have widths up to about 10 microns. Pores present in the plagioclase occur preferentially in certain compositional zones, both in the starting material (Figure 8a) and, essentially unchanged, in the experimental sample. The pores in K-feldspar and quartz can be divided into two types; isolated pores and pores associated with cracks. The pores associated with cracks tend to be elongate parallel to the plane of the crack (Figure 7).

Crack Filling

SEM observations on NWD 2200 indicate that most cracks are filled along some portion of their length. For any given crack, there is a large variability in the amount of filling present, both for cracks near the borehole and near the outer edge. Due to this variability we were not able to determine quantitatively the fraction of cracks that are filled. Cracks in an area of quartz grains near the outer edge of the specimen are predominantly filled (Figure 11b) whereas somewhat more than half of the total crack length examined in the area nearest the borehole is open (Figure 6c, 6d). However, the area located 5 mm from the borehole appeared to have a greater fraction of filled cracks than the area 1 mm from the borehole.

Outer Edge

Stereo pair SEM micrographs taken at crack intersections near the outer edge indicate that the filling material is not massive but consists of a series of plates separated by cavities. The stereo pairs were especially important in identifying holes in the filling and determining topographic relations between the filling in the cracks and that in the triple junctions. Stereo pair SEM micrographs were prepared for intersections labeled B and D in Figure 5. In these intersections (Figure 11a) the filling is topographically lower than the filling in the cracks (Figure 11b). It is platy and contains small cracks (Figure 11a). In the center of Figure 11a there is a dark area which, in the stereo view, is clearly a hole through the uppermost layer of filling material to a cavity underneath. Other plates of filling, within this cavity, are visible through the hole. The filling in the intersection in

Figure 12a also has a platy appearance with a hole to a cavity underneath the top layer. This plate-and-void structure is not apparent within cracks except in the associated pores where the crack width increases to several microns (Figure 12b).

The composition of the fillings was determined along cracks (intragrain and grain boundary) for quartz grains only, in order to minimize the uncertainties due to cations in adjacent minerals. We do not presume that the compositions of crack fillings in minerals other than quartz are necessarily the same as those for nearby quartz. In fact, Morrow et al. (1981) found that mineral fibers on fractured surfaces had compositions that were specifically related to the mineral host. The filling within the cracks near the outer edge of NWD 2200 is predominantly Si-rich. In places, the filling contains some Ca and presumably Si as indicated by an energy dispersive x-ray spectrum taken along a crack in quartz (Figure 13a). Several other cracks contain pure silica fillings, at least within the limited resolution of this technique (Figure 13b). Sometimes Mn and/or Fe are present as minor constituents. The peak heights, however, are not reliable indicators of quantity because the contributions of adjacent grains to the spectra are not known. In some areas, the cerium from the polishing compound was detected. The fact that aluminum was only once found in cracks in the samples polished with Ce_2O_3 implies that the aluminum detected in many of the cracks in the crack sections is from the polishing compound. All the EDAX spectra in Figure 13 are from samples polished with Ce_2O_3.

Borehole Area

Some cracks in the region immediately adjacent to the borehole have a massive filling. However, the filled cracks are frequently interrupted by open cracks (Figure 14a). These open cracks often have a drusy surface coating. The open cracks comprise at least 50% of the total crack length near the borehole (Figure 14b). This estimate does not take into account cracks that were too small to be observable in the 100X, mosaic micrographs. This estimate could also be in error because of the possibility that some filled cracks near the borehole were not distinguishable from the grains themselves. The Si-rich fillings in cracks near the borehole are often topographically at the same level as the polished surfaces of the grains (Figure 14a, filled portion). As a result, these filled cracks were difficult to distinguish at 100X in the SEM which may account for the apparently lower crack density. The filling itself may be cracked (Figure 15a), but such cracking may well be related to depressurization and removal of the sample after the experiment. Massive Ca-rich fillings are common in the area 5 mm from the borehole (Figure 15b).

The filling in cracks from both areas near the borehole varies more in composition than the filling at the outer edge. Material containing both Ca and Al (Figure 13c) and an almost pure Ca filling (Figure 13d) are present. These two types of filling were found within 500 microns of each other in neighboring quartz grains. Other quartz grains contained cracks with almost pure silica fillings.

DISCUSSION

The starting material contains low aspect ratio cavities (called cracks here) with some isolated bridges (Sprunt and Brace, 1974). The average length of the cracks is about 1/10 of the grain size (Sprunt and Brace, 1974). This was confirmed by Hadley (1976) who also noted that transgranular cracks are rare. Hadley (1976) defined crack lengths to be those straight sections of open crack which were separated by at least three crack widths of filling. Thus, the cracks she dealt with were, by definition, open. However, many cracks in sample NWD 2200 contained a filling that was precipitated during the experiment. Therefore, a direct comparison of crack lengths in this specimen with those determined by Hadley is problematical because it is not possible to know, from the published statistics, how many straight sections might be lined up and separated by bridges a few microns long. These would be counted as separate cracks. However, after the experiment, the original bridges might not be distinguishable from the rest of the filling. Alternatively, the original bridges may have been completely dissolved prior to precipitation of the filling. Thus, to the extent that Hadley (1976) and Sprunt and Brace (1974) measured such cracks, their determinations of maximum length would be systematically lower. Furthermore, Bruner (1984) suggests that Hadley's technique of considering bridges that were more than three crack widths long to be crack terminations may result in an underestimate of crack length. Bruner believed this could explain the discrepancy between measured and calculated p-wave velocities found by Hadley (1976).

We did not make measurements of crack length but noticed that maximum crack length in both the starting material and the NWD 2200 sample must have been larger because transgranular cracks are common if the crack bridges are ignored. For the experimental sample, this discrepancy in crack length may not be caused solely by ambiguities in the definition of cracks. Some of the difference may be due to the formation of new cracks during pressurization and/or heating. Certainly one would expect growth of cracks, especially in the region near the borehole where the temperature change was greatest and occurred most rapidly. Thermal expansion of the fluid in existing cracks was probably the dominant factor in crack growth, with anisotropic thermal expansion of minerals also a likely contributing factor. The density of transgranular cracks appeared to be higher near the outer edge of the NWD 2200 sample than the density in our sample of the starting material. This may be a result of the sample preparation or of thermal stresses during the experiment. However, the density of transgranular cracks near the borehole appeared to be less, perhaps because of the difficulty in distinguishing cracks filled with an Si-rich material. Alternatively, cracks near the borehole may have been closed by crack healing (Smith and Evans, 1984).

The intragranular cracks in quartz grains frequently intersect each other and the cracked grain boundaries (Figure 5). The feldspars exhibit a somewhat lower density of large, intragranular cracks and almost no cracks along grain boundaries with other feldspars. The grain boundaries between feldspars did not crack open during the experiment. Thus, the regions containing quartz should be substantially more permeable due to this difference in crack distribution. If the quartz forms continuous pathways through the rock, then the

permeability is likely to be greater than if it occurs only in isolated clusters. Therefore, the geometrical distribution of the major phases could be an important factor in determining the permeabilities of granitic rocks. In Westerly Granite, the inhomogeneities in mineral distribution are on the scale of several grains; as a result, the crack distribution measured by Hadley (1976) may be biased if the area chosen was not representative. Because Hadley (1976) did not distinguish among the various minerals, potential effects of variations in the distribution of cracks cannot be ascertained from the statistics.

In order to model numerically a physical property such as permeability in a rock in which the fluid pathways are narrow cracks, one must specify a model for the geometry of the cracks. This is quite difficult if there are substantial variations in the size of cracks. One approach is to determine the overall permeability for a series of embedded networks (Madden, 1976). In this model, each network interacts with networks of larger and smaller size in the same way. Permeability is calculated as an aggregate property of many such embedded networks. The observations that we have made suggest, however, that the nature of the interaction with the grain scale network will be different from interactions between networks of smaller size because of the inhomogeneities in crack distribution.

In addition to the low aspect ratio cracks, pores with roughly equal dimensions are present. In quartz and in K-feldspar these pores appear to be concentrated along cracks, in which case we have identified them as being "associated with" the cracks. Commonly such pores are slightly elongate parallel to the plane of the crack (Figure 7) and may represent cross-sections through microtubules which commonly occur in granites as a result of crack healing processes. Pores are much more numerous in plagioclase, making it difficult to distinguish those which may have formed during the experiment from those which were initially present along the cracks. Most pores probably represent fluid inclusions (Montgomery and Brace, 1975) but some may be due to plucking out of solid mineral inclusions during the grinding process.

The filling material within cracks near the borehole varied in its texture from a minor drusy surface coating in the majority of the cracks to a massive deposit. Both silica-rich and calcium-rich deposits occur as massive fillings in cracks near the borehole. The calcium-rich filling is probably calcite. The presence of calcite filling near the borehole is not surprising because calcite that was replacing plagioclase in this region was much more etched than in the starting material (Moore et al., 1983). This suggests that some of the calcite in the starting material dissolved during the experiment and may have been precipitated locally in the cracks. In natural hydrothermal systems both analcime and calcite have been found filling fractures in the same rock (Batzle and Simmons, 1976), an occurrence that was attributed to time-varying fluid chemistry. Our results indicate that two distinctly different types of filling, one silica-rich with possibly some Al and the other, apparently calcite, can be deposited under the same externally imposed conditions of confining pressure, temperature, pore pressure and pore pressure gradient because both of these fillings occur in close proximity near the borehole. Despite these constant conditions, the composition of fluids

discharged from the specimen varied with the flow rate and therefore time (Moore et al., 1983). Also, the concentrations of some species increased or decreased steadily during the experiment while others exhibited maxima or minima. Any rationalization of these temporal variations must take into account the dilution of fluids discharged early in the experiment by fluids existing initially in the space between the sample and the jacket. However, the variations of fluid composition in the latter portions of the experiments indicate that some temporal changes had been occurring in fluid composition within the samples. These observations illustrate the complexity of chemical behavior of the fluids even under constant imposed conditions.

It is difficult to predict the composition of fluids within the intact sample because, (1) the composition of the fluid entering the sample is not well known and, (2) the fluid composition within the sample changes as a result of dissolution and precipitation of minerals. The fluid being pumped into the borehole was deionized water. During its residence time in the borehole the silica concentration may have increased due to dissolution of quartz grains on the borehole surface or, possibly, dissolution of the amorphous silica endpieces. The extent to which this occurred is unknown.

Figure 16 shows plots of the equilibrium silica concentration as a function of radius in sample NWD 2200. The equilibrium curve marked F & P (1982) is taken from calculations utilizing estimated temperatures in the sample and the solubility of quartz (Fournier and Potter, 1982). The curve marked R & B (1980) is a similar plot utilizing an expression for the solubility of quartz given by Rimstidt and Barnes (1980). Estimated temperatures are also plotted against radius in the sample. There is a substantial discrepancy between the two equilibrium curves at temperatures of 200-300°C but at lower temperatures the agreement is good. Some disagreement is expected because the solubilities based on Fournier and Potter's (1983) expression are a function of specific volume as well as temperature. Based on the plots in Figure 16, the concentration of silica in fluids entering the sample will increase towards the equilibrium boundary.

The kinetics of quartz dissolution and precipitation reactions (Rimstidt and Barnes, 1980) may be used to determine the silica concentration of fluid within the sample given some assumption of the starting composition within the borehole. We have made such calculations, and the resulting fluid composition as a function of radius is plotted in Figure 17. We used an iterative procedure which is described in Appendix A. The run conditions of NWD 2200 (Table 1) were utilized for the plots in Figure 17. An initial silica content of zero was chosen for the fluid in the borehole. This fluid was progressively moved through the sample, which was divided into 20 concentric cylinders. The residence time in each hypothetical cylinder varied depending on the local fluid velocity, which is inversely proportional to the radius. Curve A represents a 1-hour total fluid residence time in the sample. This residence time, as calculated from equation 4 in Appendix A, is representative of the early stages of experiment NWD 2200. Along curve A, the silica content changes from zero to more than 300 mg/L in a matter of minutes as the fluid moves into the sample. The silica content reaches a maximum after the fluid has traveled about 5 mm into the sample. This maximum corresponds to the crossing of the

equilibrium solubility curve (labeled C in Figure 17; Rimstidt and Barnes, 1980). Further movement of the fluid outwards in the sample causes a reduction of the fluid's silica content, but the equilibrium curve, C, falls off much more sharply. Thus, the fluid has progressively greater degrees of supersaturation up to its final silica content, 222 mg/L. The curve marked B in Figure 17 represents the progressive variation of silica content for a fluid residence time of 24 hours which is characteristic of the latter portion of NWD 2200. Again, the silica content changes very rapidly near the borehole to meet the equilibrium curve, but the velocity of the fluid through the sample after saturation is slow enough that the silica content deviates only a small amount from the equilibrium curve. Figure 17 demonstrates that variations in the fluid residence time caused by, for example, variations in effective pressure or by a progressive reduction of permeability can cause significant changes in the silica content of the discharged fluids.

The concentrations of silica in the fluids discharged from NWD 2200 average about 50 mg/L, whereas the average for experiment NWD 2100 (labeled W250 in Moore et al., 1983) is about 210 mg/L (Moore et al., 1983). It is of interest to determine whether this difference can be due to variations in the fluid residence time alone or whether some other variables must be introduced. For this calculation, the residence times for the two experiments were calculated from equation 4 in Appendix A from flow rates measured during the period of 48 to 72 hours after the temperature was raised. The residence time for NWD 2100 was 2.0 hours and that for NWD 2200 was 5.7 hours. The two A/M (area of reacting surface/mass of water) ratios are 2500 and 3330 for NWD 2100 and NWD 2200, respectively. These values reflect the calculated difference in crack width based on the variation in crack porosity at the two effective pressures. The crack porosities are 1.2×10^{-3} and 0.9×10^{-3} for NWD 2100 and NWD 2200 respectively. These numbers were obtained by adjusting the initial crack porosity (2×10^{-3}; Brace et al., 1968) to account for the closure of cracks by the effective pressure. Low pressure bulk moduli from Brace et al. (1968) were used giving a value of 0.9×10^{-3} for the initial crack porosity at 40 MPa effective pressure.

Two numerical integrations of equation 3 (Appendix A) resulted in final silica concentrations of 165 mg/L in run NWD 2100 and 65 mg/L in NWD 2200. Therefore, the variation of fluid residence time accounts for about 60% of the difference in silica concentration. Two potential sources of the discrepancy between observed and calculated silica concentrations are: (1) possible differences in the A/M ratio between the two experiments that are not simply caused by the closure of cracks at different effective pressures, (2) fundamental changes in the crack characteristics perhaps due to crack healing which could be enhanced in the higher temperature experiment (NWD 2200).

Variations in the silica contents of the fluids within the sample reflect dissolution or precipitation of silica and other silicate minerals in cracks. The crack porosity of the sample is therefore being changed locally due to these processes. Figure 18 plots the cumulative effect of both dissolution and precipitation as a percentage of initial crack porosity (0.9×10^{-3}) for conditions in the NWD 2200 experiment. The calculation of the amount of quartz precipitated in NWD 2200 as a function of radius is similar to that for the evolution of fluid compositions (Figure 17). Because fluid residence time

changed during the experiment, the cumulative effect was determined by running small amounts of fluid through the hypothetical sample until the sum of these small amounts was equivalent to the total discharge from the actual sample. A new residence time was utilized for each incremental amount of fluid that flowed through. Residence times were obtained from equation 4 in Appendix A with the flow rate, Q, calculated from a 6th order polynomial that was fitted to the data. A summation of the amount of silica dissolved or precipitated was maintained for each hypothetical concentric cylinder of the rock as the successive increments of fluid moved through. The result of this calculation is that, in comparison to the crack porosity, very little material was deposited in the sample. The maximum deposition is about 8% of the crack porosity at a distance of 3 mm from the borehole (Figure 18). To estimate the effect of this deposit on permeability, we utilize an equation relating permeability and crack porosity, $k = (m^2/A)\phi^3$ (Brace, 1977). In this equation, A is a constant, m is hydraulic radius and ϕ crack porosity. We assume that filling less than 10% of the porosity will not change the hydraulic radius significantly. This assumption is valid if the precipitated quartz coats all of the cracks in the sample evenly which may not be the case in our experimental sample. An even coating will be similar in its effect on permeability to the application of confining pressure. Brace (1977) has argued that, for Westerly, the hydraulic radius is independent of effective confining pressure. Therefore, the variation in permeability is proportional to the cube of the porosity change. For the 8% maximum porosity change calculated for NWD 2200, the reduction in permeability is 22%. Thus, this simple precipitation mechanism, in which quartz coats each crack uniformly, can account for about a fourth of the observed permeability reduction of 96%. Other factors that may be important in the permeability reduction are: (1) crack healing, (2) non-homogeneous precipitation of quartz, (3) non-homogeneous precipitation of other minerals such as calcite and zeolites. Either of the last two possibilities might result in the formation of discontinuous crack fillings which effectively seal the rock without constituting a volumetrically significant portion of the crack porosity.

CONCLUSIONS

During a permeability experiment in which heated water was forced through a cylindrical sample of Westerly Granite in a radial direction down a temperature gradient (300°C - 92°C), the measured permeability dropped by a factor of about 25. The reduction of permeability in this experiment has been attributed to the dissolution and reprecipitation of minerals on crack surfaces (Moore et al., 1983). The work reported here focused on the crack characteristics of the sample and especially the crack fillings. Fillings in cracks in quartz immediately adjacent to the borehole consist of varying proportions of Ca and Si and even a small amount of Al. Nearly pure silica fillings are common near the cooler, outer edge of the sample. Most cracks near the outer edge of the sample are filled, whereas at least 50% of cracks in the areas near the central borehole are open. Most large cracks in quartz, whether open or filled, have rough surfaces, suggesting that dissolution occurred at some point during the experiment. Some of this dissolution may have occurred during the initial heating when fluid residing in the sample was everywhere undersaturated.

The distribution of cracks in the intact sample is not completely homogeneous. Grain boundaries surrounding quartz are usually cracked open or have been cracked open at some time and subsequently filled. However, grain boundaries between the two feldspars are only rarely cracked open both in the starting material and in the intact experimental sample. Thus, the fluid pathways are more effectively connected in the regions containing quartz. The geometrical distribution of quartz would seem to be important in determining the permeability of granitic rocks.

The chemical composition of fluids discharged from the sample has been determined by analyzing fluids that were withdrawn from the sample at several times during the experiment (Moore et al., 1983). Silica contents of discharged fluids measured for the experiments NWD 2100 and NWD 2200 were 210 and 50 mg/L, respectively. The fluid residence times were 2.0 hours for NWD 2100 and 5.7 hours for NWD 2200 with the higher effective pressure causing the longer fluid residence time. We have developed a simple numerical integration routine to calculate the silica contents of fluid in the sample as a function of radius. This calculation is based on kinetic equations for silica dissolution and precipitation (Rimstidt and Barnes, 1980). The variation in fluid residence time between these two experiments can account for about 60% of the observed variation in silica content of the discharged fluids. An additional factor that may contribute to the observed variation is a potential change in the A/M (area of reacting surface/mass of water) ratio for cracks with time resulting in more efficient precipitation.

We have also calculated the total amount of silica precipitated in the samples based on Rimstidt and Barnes' (1980) rate equations. Calculations for NWD 2200 indicate that the maximum volume of quartz precipitated accounts for 8% of the crack porosity at a distance of 3 mm from the borehole wall. Utilizing a relation between crack porosity and permeability (Brace, 1977) we find that a simple solution-precipitation model of crack sealing, in which the precipitating quartz uniformly coats the cracks, can account for 22% of the observed 96% permeability reduction in the NWD 2200 experiment. This result differs from that obtained by Keith et al. (1985), in that they calculated a greater permeability reduction than actually observed. The reason for this discrepancy is not immediately apparent.

A second potential mechanism that could contribute to the observed permeability reduction is crack healing. Crack healing can reduce crack porosity by the dissolution and reprecipitation of quartz on a local scale within cracks (Smith and Evans, 1984). The reprecipitation during crack healing occurs in crystallographic continuity with the surrounding grain. A third possible effect that could reduce permeability is due to the geometrical characteristics of the material precipitated. The precipitates may have effectively closed off cracks by forming bridges. Thus, even though the total amount of precipitated material might be small, the net effect on permeability could be large. SEM observations tend to support both of these additional sources of permeability reduction. The low crack density near the borehole suggests crack healing. The platy texture near the outer edge and the occurrence of open cracks interrupted by massive fillings near the borehole both indicate inhomogeneous precipitation. The precipitation of calcite,

which appeared to be greater in areas near the borehole may have made important contributions to the permeability reduction. Finally, the precipitation of other minerals such as zeolites could be important especially in the cracks in feldspars where locally higher Al concentrations may have occurred in the fluids.

APPENDIX A

The rate equation for dissolution and precipitation of silica (Rimstidt and Barnes, 1980) can be applied to our experiments by calculating the changes in silica content that occur as the fluid is subjected to a series of temperature variations designed to simulate its movement through the real sample. The two most important variables in this problem are the temperature, which is a function of the radius in the sample (Figure 16), and the local fluid residence time. The local rate of change in fluid composition may be obtained from the rate equation,

$$\frac{dm}{dt} = (A/M)(k_+ - k_- m) \tag{1}$$

where m is the molal concentration of H_4SiO_4 in solution; A/M is the ratio (area of reacting solid/mass of water); k_+ and k_- are the rate constants for dissolution and precipitation respectively. This equation was obtained by Rimstidt and Barnes (1980) under the assumption that the activity coefficient, $\gamma_{H_4SiO_4}$, a_{SiO_2} and a_{H_2O} are all constant and are therefore included in the rate constants. The A/M ratio can be calculated from an assumption of the crack width (Rimstidt and Barnes, 1980). For the calculations discussed in this paper, the assumed width is 1 micron, giving an A/M ratio of 2500.

Equation 1 has the solution,

$$m(t) = k_+/k_- + (m_0 - k_+/k_-)e^{-(A/M)k_- t} \tag{2}$$

where m_0 is the starting concentration. Because the temperature is not constant in the sample, the silica content of the fluid varies with radius and must be calculated iteratively using equation 2, with changing values of the two rate constants and the local residence time. For the calculation, the sample is divided up into a series of 20 concentric cylinders and the silica content of the fluid was recalculated in each one. Thus,

$$m_i = k_+/k_- + (m_{i-1} - k_+/k_-)e^{-(A/M)k_- t} \tag{3}$$

where m_{i-1} refers to the concentration of H_4SiO_4 in the fluid in the cylinder immediately within cylinder i.

During each experiment a known amount of fluid passed through the sample. Because the total fluid residence time increased as the experiment progressed, the calculation of the amount of quartz deposited required the total amount of fluid to be represented as the sum of small increments. Each of these increments corresponded to a particular global fluid residence time. By calculating the amount of material dissolved or precipitated in each hypothetical cylinder of the sample for each increment of fluid that passes through, one can obtain the local change in crack porosity. The crack porosity for Westerly Granite

is 2×10^{-3} (Brace et al., 1968). This has been adjusted to account for reduction of porosity due to the effective pressure by using low pressure bulk moduli (Brace et al., 1968). The result is an initial crack porosity of 0.9×10^{-3} at an effective pressure of 40 MPa . The sum of changes in porosity due to dissolution/precipitation processes acting over the period of the experiment is indicated in Figure 18 as a percentage of the initial crack porosity (0.9×10^{-3}). The residence time is related to flow rate and porosity by

$$t_{res} = \frac{2\pi h \phi (r_f - r_i)^2 \ln (r_f/r_i)}{Q} \qquad (4)$$

where ϕ is the crack porosity, r_f and r_i are the outer and inner radii, respectively, of the cylindrical sample; h is the length of the sample and Q is the flow rate. The flow rates were calculated from the continuous record of the volume of fluid that had been pumped through the sample. These rates were fitted to a 6th order polynomial to obtain a crude expression for the flow rate during an experiment. With this expression for flow rate, the residence time for fluid in the sample could be obtained easily from equation 4.

APPENDIX B

INTRODUCTION

The wafer experiment (NWD 3300) was similar to the NWD 2200 experiment except that an artificial fluid pathway was established along the interface between two polished surfaces of Westerly Granite (Figure 19). Fluid flow in this sample had two components. One was flow along the interface and the other was flow through the intact bulk sample. The wafer experiment was designed to locate areas of dissolution and/or precipitation on the polished surface. For the wafer experiment, NWD 3300, the sample assembly was the same as that for NWD 2200 but the sample itself was modified. A disc of Westerly Granite, 2.5 mm thick, that was highly polished on one side, was placed between two larger cylinders of Westerly Granite (Figure 19). The polished disc surface was matched with a polished surface on one of the large cylinders. A gold shim was placed along the other interface to restrict flow to the polished side. The thin disc was used to simplify sample preparation for SEM analysis. The NWD 3300 samples was taken from a block originating in the same quarry as the NWD 2200 sample.

OBSERVATIONS

Permeability in NWD 3300 was significantly higher than the permeability of an intact sample (Figure 2). But the permeability dropped significantly during NWD 3300 as is commonly found for the intact samples.

SEM observations were made on two 2.5 cm squares that were cut from the wafer sample (NWD 3300) without using coolant, in order to preserve any delicate structures on the surface. One of the squares was cut from an area near the borehole and a second from the outer edge of the sample. These two squares were carbon-coated but no other surface preparations were made.

The appearance of the polished surface in the SEM after the experiment suggests dissolution. The entire surface is pitted to about the same degree, with the exception of mica grains which have rounded smooth surfaces (Figure 20). The area shown is approximately 1 mm from the central borehole, but the outer edge of the wafer has an identical surface texture. The only difference in surface texture among the three major minerals is that, in some orientations, the feldspars have pits that are elongate along crystallographic directions. The pitting has obscured most other surface features with the exception of grain boundaries. However, it is not possible to determine whether or not the grain boundaries are cracked. There is no evidence of precipitation such as the presence of mineral fibers on the polished surface.

DISCUSSION - NWD 3300

The effect of introducing the polished interface was determined by comparing permeabilities in NWD 3300 and NWD 2100; experiments with identical run conditons. NWD 2100 is labeled W250 in Moore et al. (1983). The permeability in NWD 3300 was greater by a factor of 4.6 initially; this decreased to a factor of 1.7 after 9 days. Because permeability dropped by a greater

amount in NWD 3300 than in NWD 2100, it is evident that sealing processes operated along the interface in NWD 3300 in addition to those which operated in the bulk portion of the sample.

A further quantitative analysis of the effect of the polished interface on effective permeability and fluid composition requires a comparison of flow rates in the NWD 3300 sample with those for an intact sample held under identical conditions (NWD 2100). The amount of fluid discharged from the intact portion of the NWD 3300 sample can be calculated from the flow rates obtained in the NWD 2100 experiment. For this calculation, the flow rate in NWD 2100 was adjusted for the different pressure drop assuming Darcy's Law. Using the flow rate measured 3 days after the temperature was raised and comparing it with the flow rate at 3 days for the intact sample under similar conditions, the percentage of total fluid flow that occurred along the interface is 51%. Intuitively, this is reasonable because the pore pressure difference in the two experiments varies by a factor of 2 yet the flow rates are almost the same. The concentration of silica in fluids discharged from the samples NWD 2200 and NWD 2100 were, respectively, 50 and 210 mg/L. We use the following expression,

$$c_{Si,i} = (c_d Q_t - c_{Si,b} Q_b)/Q_i$$

to obtain the concentration of silica in fluids discharged from the interface. c_d is the silica concentration measured for NWD 3300; $c_{Si,b}$ is the silica concentration estimated for the fluids discharged from the intact bulk portion of NWD 3300. Q_t, Q_b and Q_i are the flow rates for, respectively, the entire sample, the intact portion and the interface. Because about 51% of the total flow occurred along the initially polished interface, we find, from the expression above, that this interfacial flow accounted for 42% of the total amount of silica removed from the sample. The pitted appearance of the initially polished interface is consistent with these calculations. What is peculiar about the condition of the surface is that pitting extends to the outer edge where calculations indicate that the fluid was supersaturated with respect to quartz, chalcedony and alpha-cristobalite (Moore et al., 1983, similar conditions as NWD 2100) throughout the experiment. This is difficult to reconcile with the other information concerning this experiment. The discharged fluids were supersaturated with respect to quartz, yet quartz appears to be dissolved even near the outer edge of the sample. The same texture appeared on the surfaces of the feldspars although the discharged fluids had very low aluminum concentrations. One possible explanation of the uniform pitting over the wafer surface is that the polishing process created a surface layer of highly soluble material. This might be an amorphous material or a gel composed of water molecules and ultrafine particles. Either could reside in extremely small surface irregularities.

REFERENCES

Batzle, M. L. and G. Simmons, Microfractures in rocks from the geothermal areas, Earth Planet. Sci. Lett., 30, 71-93, 1976.

Brace, W. F., Permeability from resistivity and pore shape, Jour. Geophys. Res., 82, 3343-3349, 1977.

Brace, W. F., J. B. Walsh, and W. T. Frangos, Permeability of granite under high pressure, Jour. Geophys. Res., 73, 2225-2236, 1968.

Bruner, W. M., Crack growth during unroofing of crustal rocks: Effects on thermoelastic behavior and near-surface stresses, Jour. Geophys. Res., 89, 4167-4184, 1984.

Fournier, R. O. and R. W. Potter, An equation correlating the solubility of quartz from 25°C to 900°C at pressures up to 10,000 bars, Geochim. Cosmochim. Acta, 46, 1969-1974, 1982.

Hadley, K., Comparison of calculated and observed crack densities and seismic velocities in Westerly Granite, Jour. Geophys. Res., 81, 3484-3494, 1976.

Keith, L., P. T. Delaney, and D. E. Moore, Permeability reduction due to precipitation of quartz under nonisothermal conditions, Proceedings of Stanford Geothermal Workshop IX, in press.

Madden, T. R., Random networks and mixing laws, Geophysics, 41, 1104-1125, 1976.

Montgomery, C. W. and W. F. Brace, Micropores in plagioclase, Contrib. Mineral. Petrol., 52, 17-28, 1975.

Moore, D. E., C. A. Morrow, and J. D. Byerlee, Chemical reactions accompanying fluid flow through granite held in a temperature gradient, Geochim. Cosmochim. Acta, 47, 445-453, 1983.

Morrow, C., D. Lockner, D. Moore, and J. D. Byerlee, Permeability of granite in a temperature gradient, Jour. Geophys. Res., 86, 3002-3008, 1981.

Rimstidt, J. D. and H. L. Barnes, The kinetics of silica-water reactions, Geochim. Cosmochim. Acta, 44, 1683-1699, 1980.

Simmons, G. and L. Caruso, Microcracks and radioactive waste disposal, in: Scientific Basis for Nuclear Waste Management Symposia VI, Materials Research Society Symposia Proceedings, 15, 331-338, 1983.

Simmons, G. and D. Richter, Microcracks in rocks, in: The Physics and Chemistry of Minerals and Rocks, R. Strens, ed., Interscience, New York, 105-137, 1976.

Smith, D. L. and B. Evans, Diffusional crack healing in quartz, Jour. Geophys. Res., 89, 4125-4135, 1984.

Sprunt, E. and W. F. Brace, Direct observation of microcavities in crystalline rocks, Int. J. Rock Mech. Min. Sci. Geomech. Abstr., 11, 139-150, 1974.

Warren, N., Characterization of modulus-pressure systematics of rocks: Dependence on microstructure, in: The Earth's Crust, J.G. Heacock (Ed.), AGU, Geophysical Monograph, 20, 119-148, 1977.

FIGURE CAPTIONS

Figure 1. Schematic of the sample assembly, showing an intact Westerly Granite cylinder as used in experiment NWD 2200.

Figure 2. Permeability (nda) as a function of time from initial heating for experiments NWD 2200 and NWD 3300. The vertical dashed lines represent times when the pore pressure fluid pump was being recharged. Some anomalous peaks occur at times when fluid was withdrawn for chemical analyses.

Figure 3. Diagram of crack section locations. The two solid circles are the inner and outer radii of the sample. The dashed circles, labeled CS, are the positions of the two crack sections. The numbers identify locations of the areas studied in detail using SEM (1:1 mm from the borehole, 2:5 mm from the borehole, 3:0.5 mm from the outer edge).

Figure 4. Starting material, Westerly Granite (SEM). A) Grain boundary between K-feldspar (K) and quartz (Q) is uncracked at this resolution. B) Intragrain crack in quartz intersecting an open crack along a grain boundary between quartz and K-feldspar. Small grains of polishing compound are visible.

Figure 5. NWD 2200, 0.5 mm from outer edge. A network of large intragrain cracks and grain boundary cracks in quartz (crack section - SEM). The intragrain cracks are marked with small arrows, all other visible cracks follow grain boundaries. A large arrow points to a place where an uncracked grain boundary exists for a short distance. The letters denote areas in which higher magnification micrographs were prepared. Some of these are shown in subsequent figures.

Figure 6. Intragrain cracks in quartz (all SEM). A) Starting material, crack containing isolated silica-rich bridges. B) NWD 2200, 0.5 mm from outer edge. Note the variation in crack width and the presence of filling. C) NWD 2200, 1.0 mm from borehole. Open cracks like this one are common near the borehole. These cracks contained fewer silica bridges than the starting material. D) NWD 2200, 5.0 mm from borehole. Open cracks like this one are not as common here as in the area immediately adjacent to the borehole. Note also the somewhat rougher crack surfaces than in the starting material.

Figure 7. NWD 2200, 3 mm from outer edge. Narrow intragrain crack in quartz with associated micropores (SEM). In certain locations this crack was so narrow that it could not be resolved using the SEM.

Figure 8. Intragrain crack in the feldspars (all SEM). A) Starting material, an intragrain crack in K-feldspar meets an uncracked K-feldspar (K) - plagioclase (P) grain boundary. B) NWD 2200, 3 mm from outer edge, crack in K-feldspar has associated pores. C) NWD 2200, 1 mm from borehole crack in K-feldspar is narrow and sinuous with no filling. D) NWD 2200, 5 mm from borehole, crack in plagioclase contains a filling. This area has a very low pore density compared to that often found in the plagioclase.

Figure 9. Plagioclase - K-feldspar grain boundaries. A) Starting material (BSE). B) NWD 2200, 1 mm from outer edge. A large open crack is present in plagioclase but does not follow the grain boundary (BSE). C) NWD 2200, 1 mm from borehole (BSE). D) NWD 2200, 5 mm from borehole (SEM).

Figure 10. NWD 2200, 5 mm from outer edge. Optical micrograph, plane light, grain boundary between quartz and plagioclase (marked GB). Parallel cleavage cracks (marked C) present in plagioclase.

Figure 11. NWD 2200, 0.5 mm from outer edge, both SEM. A) Location B in Figure 6, intersection of grain boundary cracks. The filling in this crack intersection is platy, as indicated by the dark area in the center of the micrograph, which is an opening to a cavity in the filling. B) Grain boundary crack with filling, location C in Figure 6.

Figure 12. NWD 2200, 0.5 mm from outer edge, both SEM. A) Location D in Figure 6. B) Location E in Figure 6. An enlarged space or cavity (associated pore) along a grain boundary crack between two quartz grains. The filling in both of these micrographs contains cavities.

Figure 13. NWD 2200, energy dispersive x-ray spectra from cracks in quartz: A,B) Cracks about 1 mm from the outer edge, C) Massive filling in grain boundary crack, 1 mm from borehole, D) Cracked filling with massive appearance similar to that of (C), 1 mm from borehole.

Figure 14. NWD 2200, 1 mm from central borehole, both SEM. A) Grain boundary crack with massive filling intersecting open crack with scalloped appearance, filling is Si-rich. B) Intragrain crack, open.

Figure 15. NWD 2200, cracks in quartz near borehole, Ca-rich fillings, both SEM. A) 1 mm from borehole. The crack in the filling itself (identified by arrows) may have developed during depressurization or temperature reduction at the end of the experiment (SEM). B) 5 mm from borehole. Intragrain crack with massive filling.

Figure 16. Solubility of quartz as a function of radius in the NWD 2200 experiment as calculated from empirical formulas (F & P - Fournier and Potter,1982; R & B Rimstitdt and Barnes, 1980). Points plotted are silica contents of discharged fluids and the number of days from the initial heating of the sample is indicated for each point. Temperatures in the sample are also plotted.

Figure 17. Plots of silica content of fluids in the sample as a function of radius. These plots represent the results of calculations based on Rimstidt and Barnes' (1980) rate equations as applied to our experiments. As fluid enters the sample its initial silica content is presumed to be zero. The silica content increases rapidly (curves A and B) due to dissolution of quartz. After reaching a maximum the silica content drops due to precipitation in the cooler regions of the sample. Curve A represents a total fluid residence time in the sample of one hour, curve B is for 24 hours. Curve C is the equilibrium solubility of quartz. These fluid residence times are characteristic of the early and late portions of the experiment NWD 2200. A complete discussion of the calculations is contained in Appendix A.

Figure 18. This plot represents the amount of quartz deposited in sample NWD 2200 as a percentage of the available crack porosity. The calculation is based on Rimstidt and Barnes' (1980) rate equations and is discussed in detail in Appendix A. The region of maximum deposition is located close to the borehole but the amount of quartz deposited is less than 10% of the available crack porosity.

Figure 19. Schematic of sample configuration for wafer sample experiment (NWD 3300). Portions of the sample assembly that are not shown are identical to Figure 1.

Figure 20. NWD 3300, SEM, this surface was initially polished, but, after the permeability experiment, both quartz (upper left) and plagioclase (right side) are pitted. The biotite is smooth and rounded. This surface texture extends over the whole area from the borehole to the outer edge.

TABLE 1

Experimental Conditions and Permeabilities

	NWD 2200	NWD 3300
Confining Pressure (MPa)	60	30
Pore Pressure (MPa)	20	10
Pore Pressure Difference* (MPa)	1.0	0.25
Temperature, Borehole (°C)	300	250
Temperature, Jacket (°C)	92	81
Duration of Run (Days)	13	22
Initial Permeability (nda)	243	3400
Final Permeability (nda)	9.3	71

* As measured between the borehole and the jacket

TABLE 2

Chemical Analyses of Discharged Fluids (mg/L)

Run #	Time (days)	pH	SiO_2	Na	K	Mg	Ca	Al	HCO_3	SO_4	F	Cl	Balance (%
NWD 2200	1.0	7.6	47	62	32	4.4	91		300	36	3.8	91	-5.6
	3.1	7.6	59	76	33	6.4	87		340	66	3.6	87	0.2
	3.9	7.2	58	81	36	6.1	77		320	66	3.3	77	-4.9
	4.9	7.0	69	81	37	7.5	73		350	70	3.5	73	5.6
	8.0	7.6	34	78	41	6.8	64		320	60	3.6	64	4.8
NWD 3300	3.0	7.3	180	36	15	2.3	32	0.01	140	12	3.7	30	3.7
	4.9	6.9	200	38	12	2.0	33	0.02	150	11	3.7	26	3.6
	7.9	6.7	150	40	13	2.3	33	0.01	180	11	4.1	23	-3.4
	16.0	6.9	160	48	13	2.5	41		220	12	4.9	21	-0.7
	19.0	6.8	160	48	12	2.3	37	0.01	220	10	5.0	17	-2.8
	21.9	6.8	160	48	11	2.1	35		220	9	5.0	12	-2.4

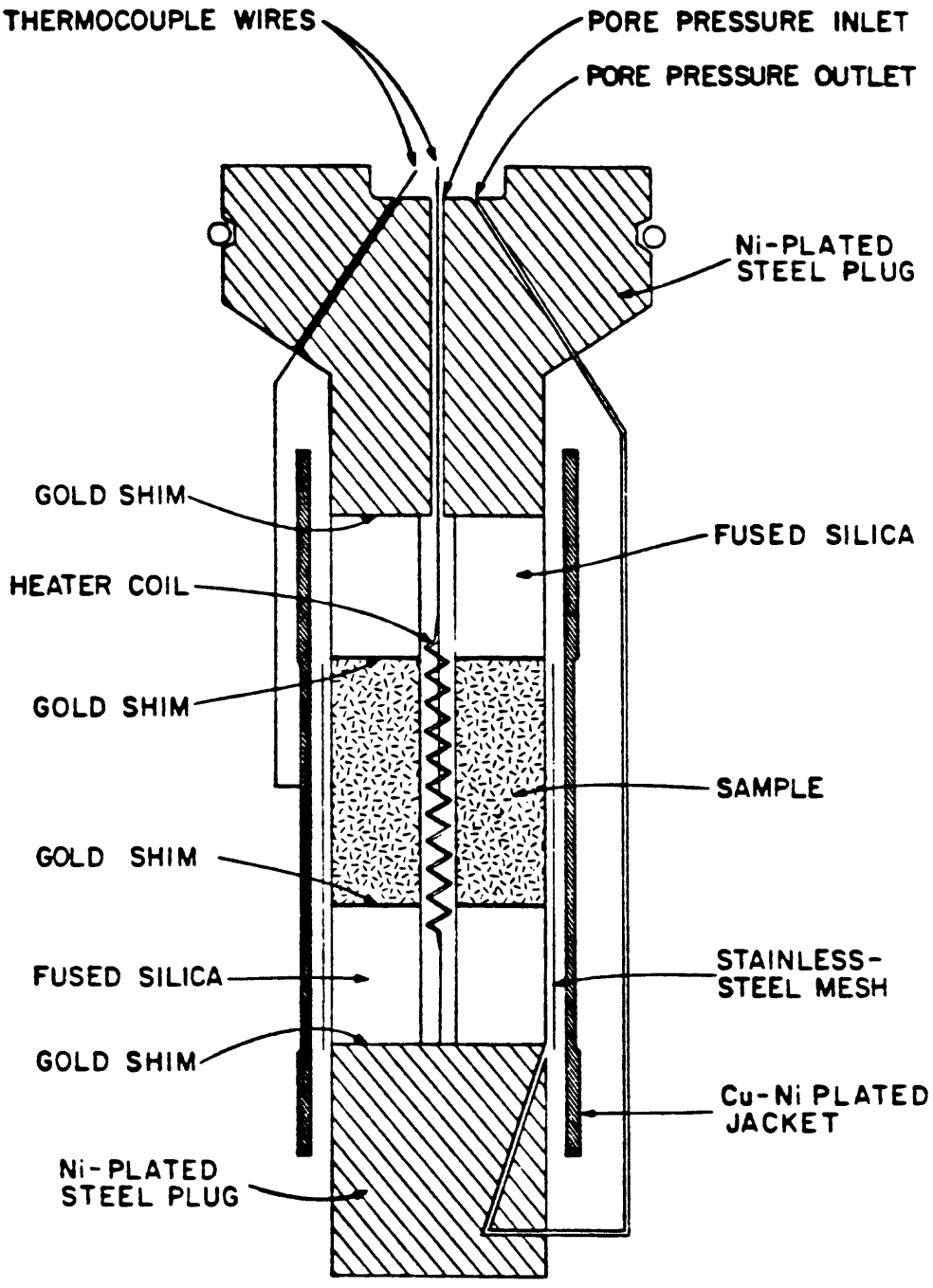
THERMOCOUPLE WIRES
PORE PRESSURE INLET
PORE PRESSURE OUTLET
Ni-PLATED STEEL PLUG
GOLD SHIM
FUSED SILICA
HEATER COIL
GOLD SHIM
SAMPLE
GOLD SHIM
FUSED SILICA
STAINLESS-STEEL MESH
GOLD SHIM
Cu-Ni PLATED JACKET
Ni-PLATED STEEL PLUG

Figure 1.

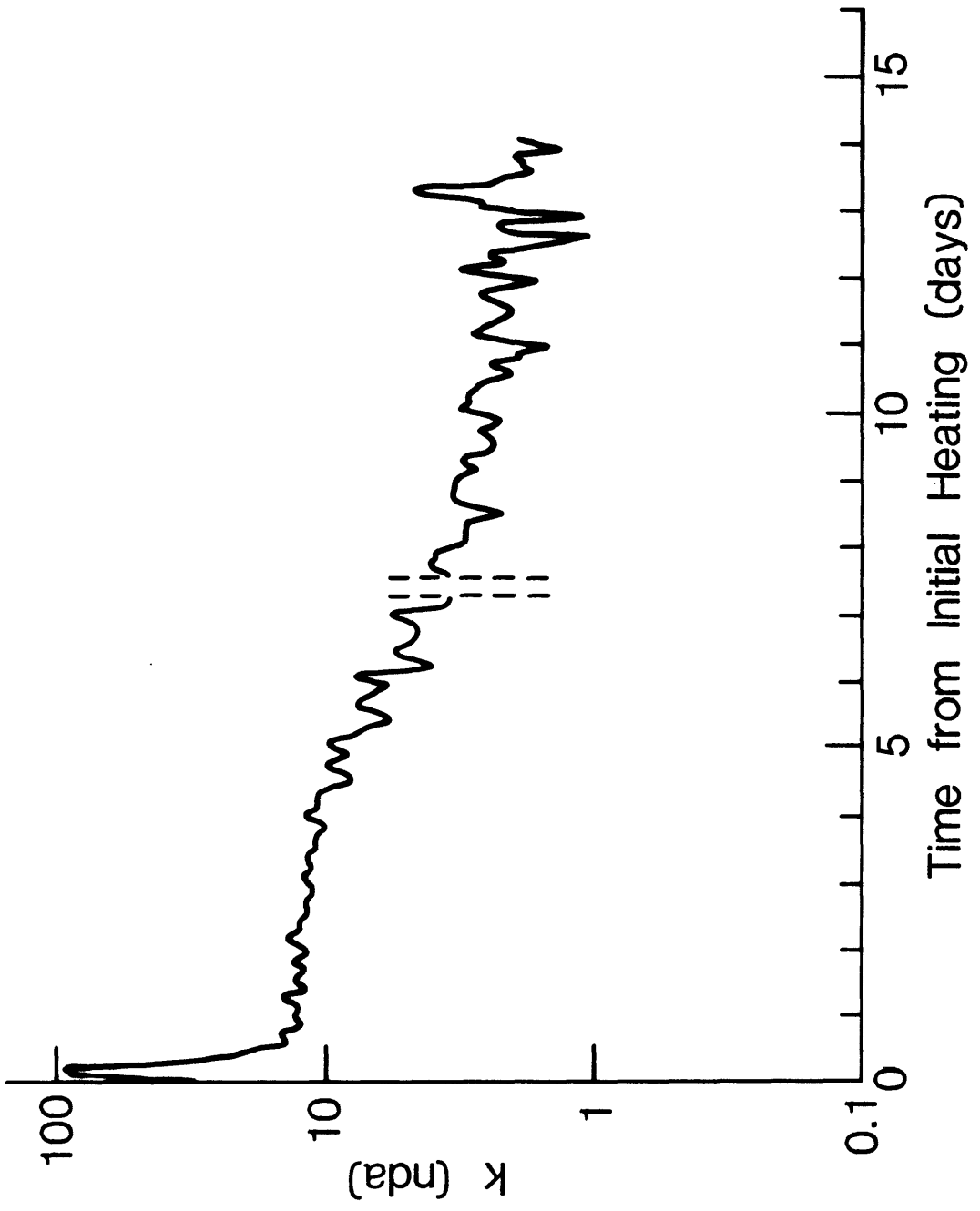

Figure 2.

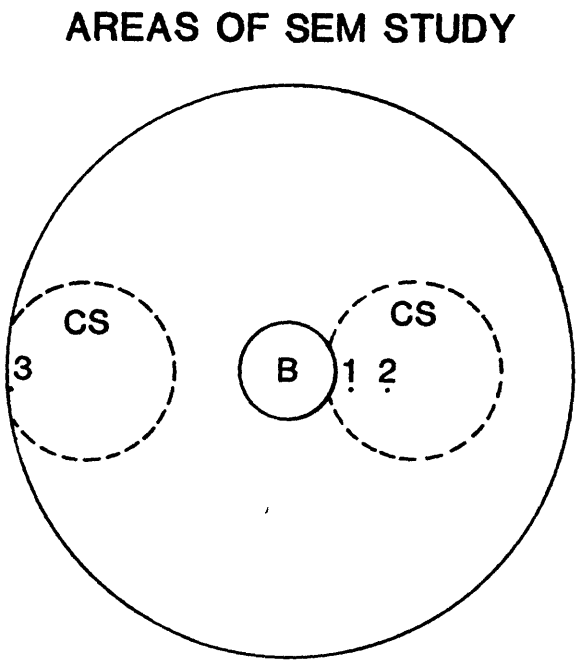

Figure 3.

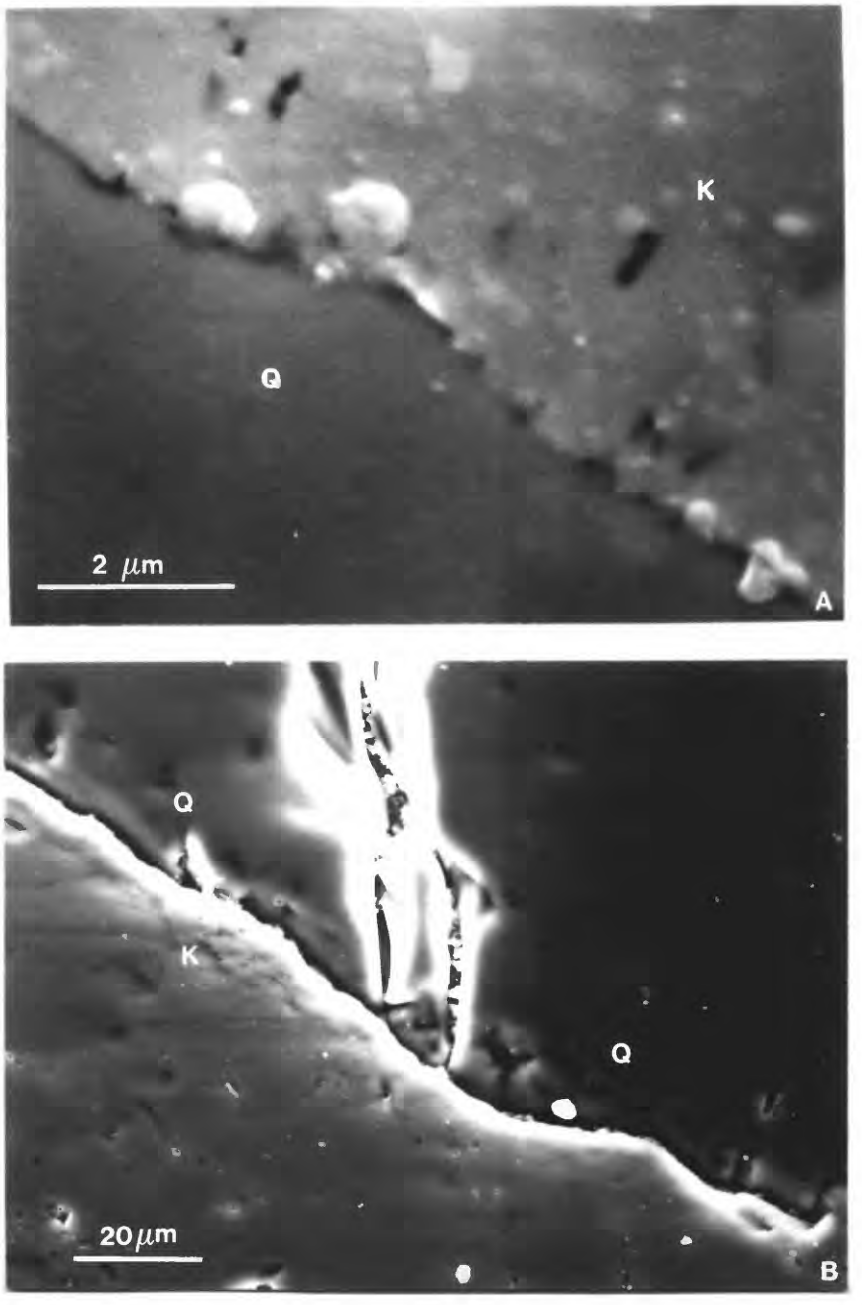

Figure 4.

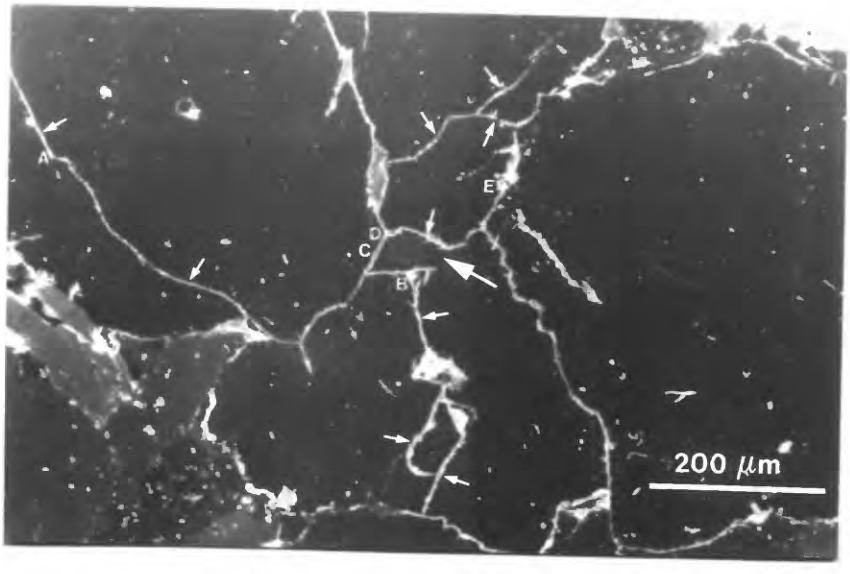

Figure 5.

Figure 6.

Figure 7.

Figure 8.

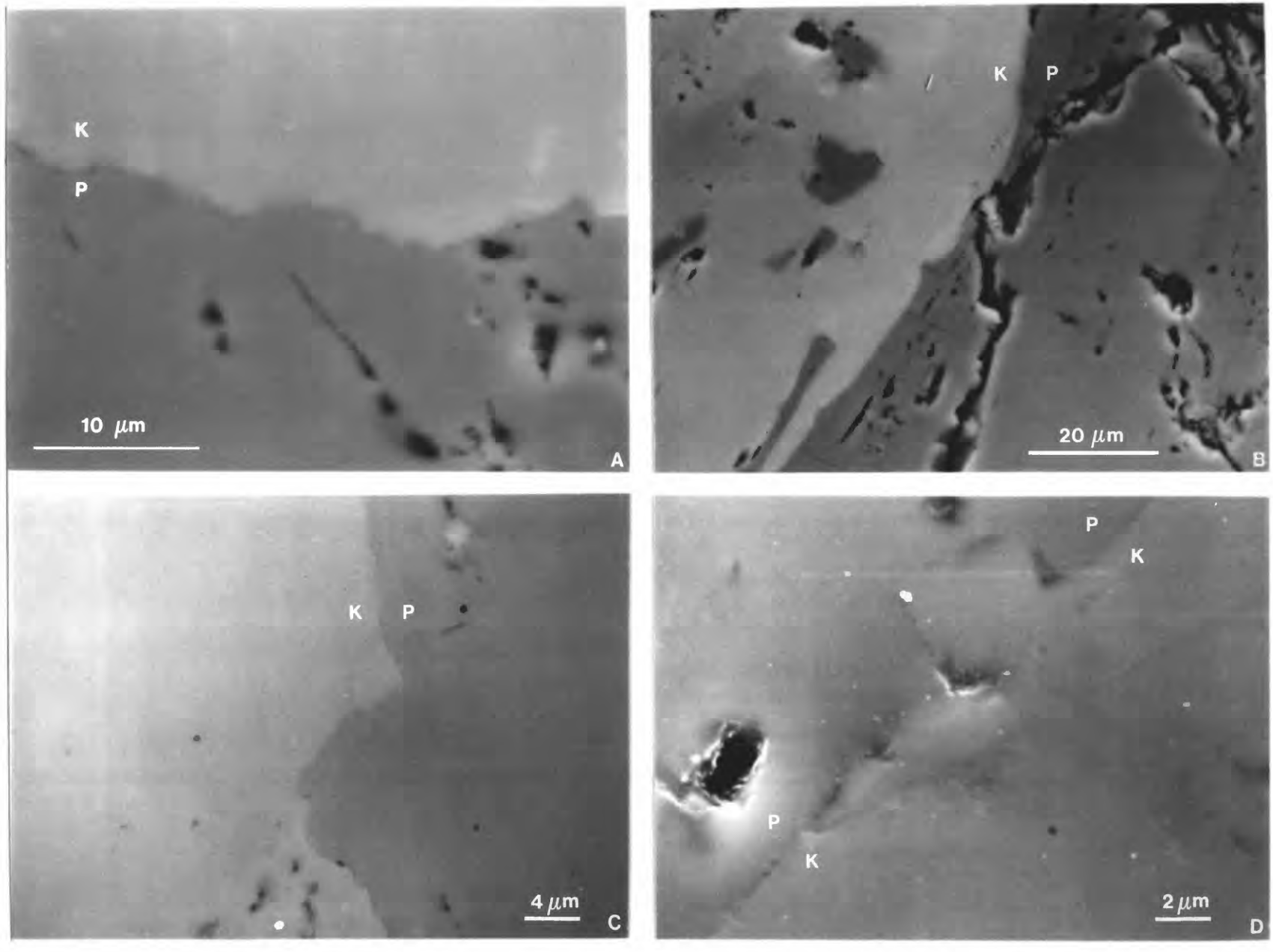

Figure 9.

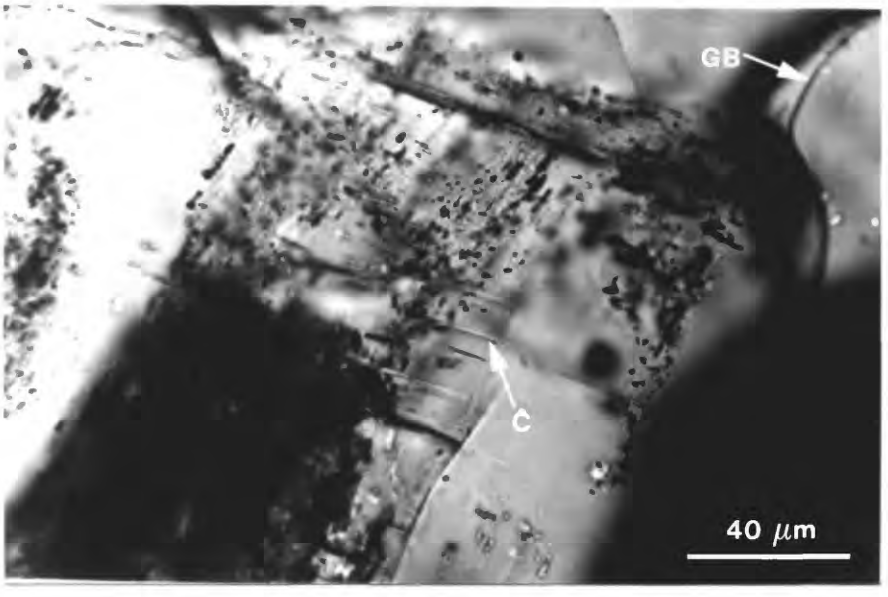

Figure 10.

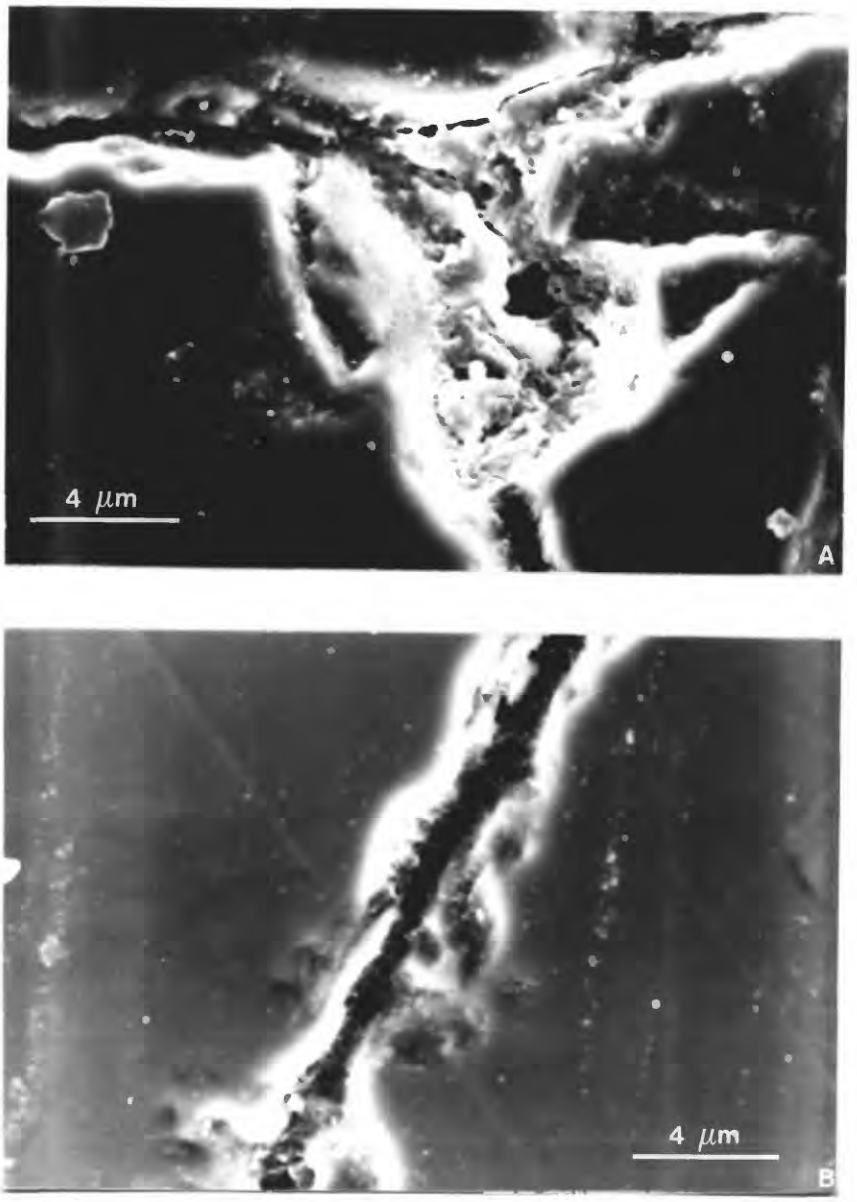

Figure 11.

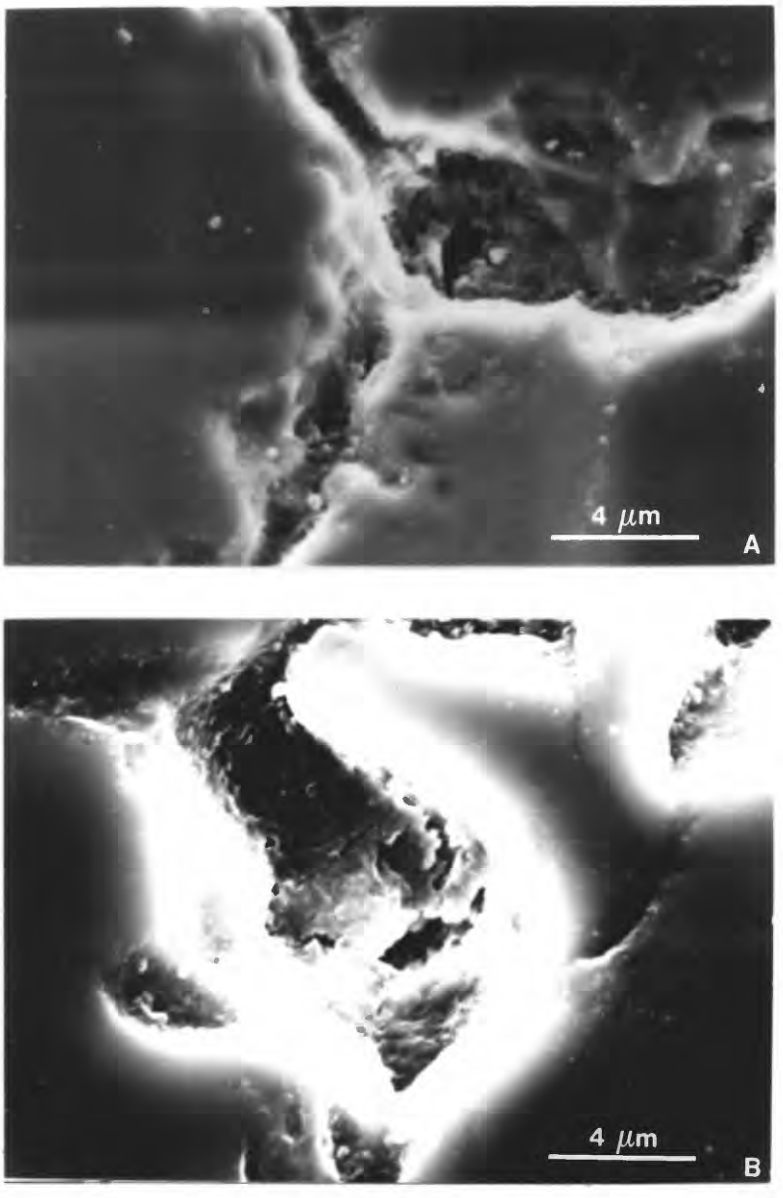

Figure 12.

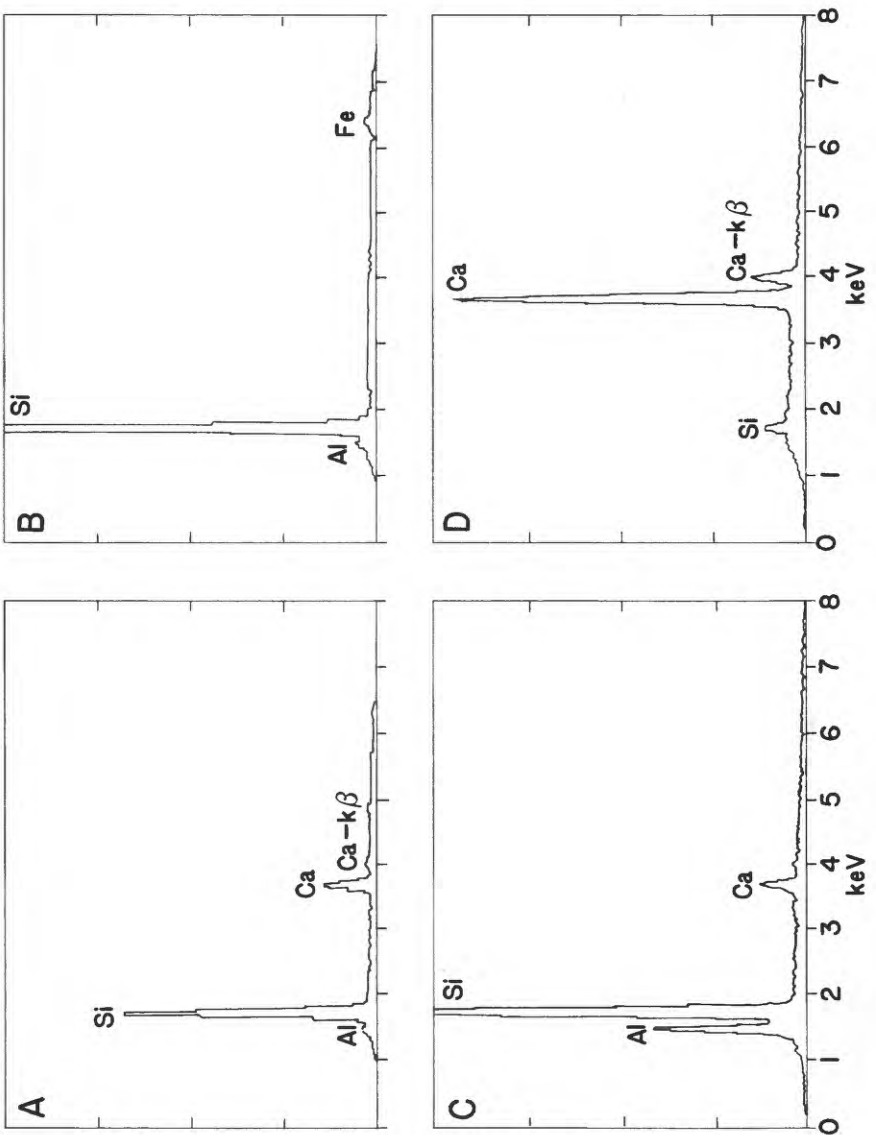

Figure 13.

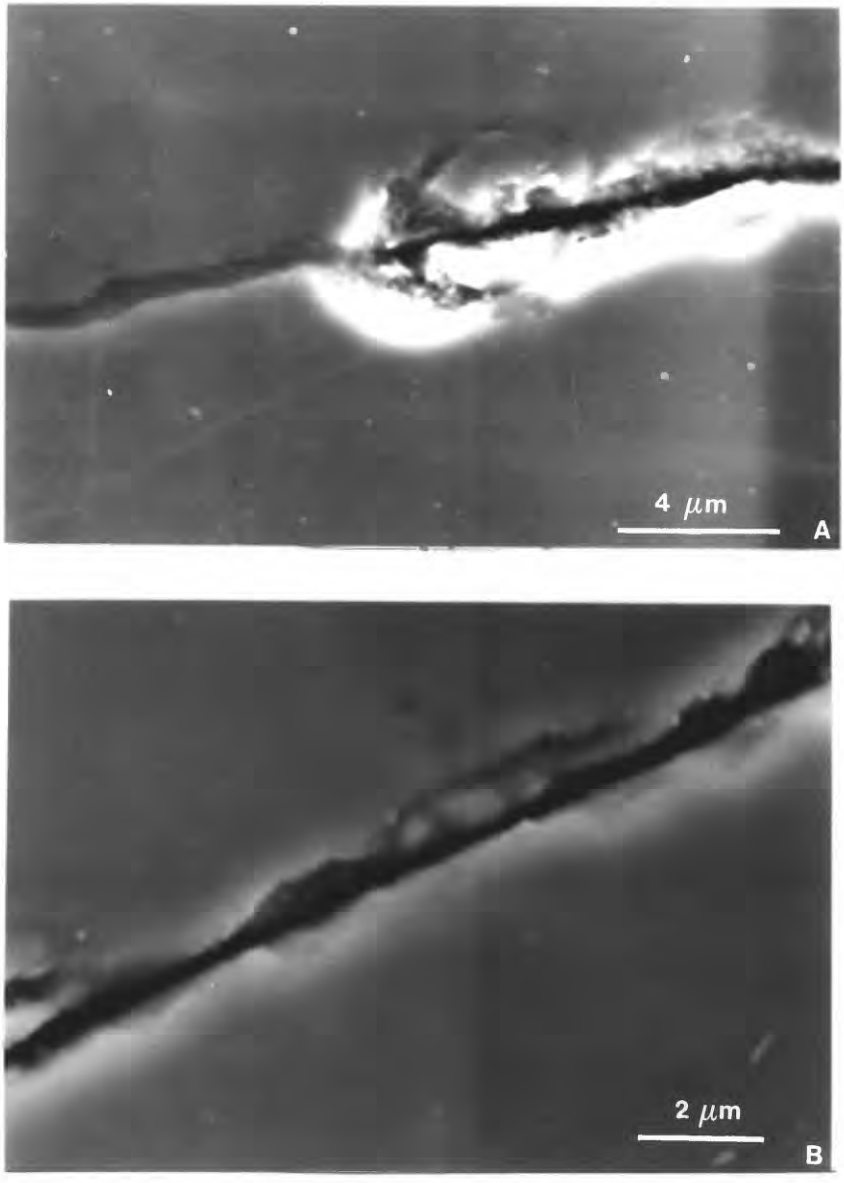

Figure 14.

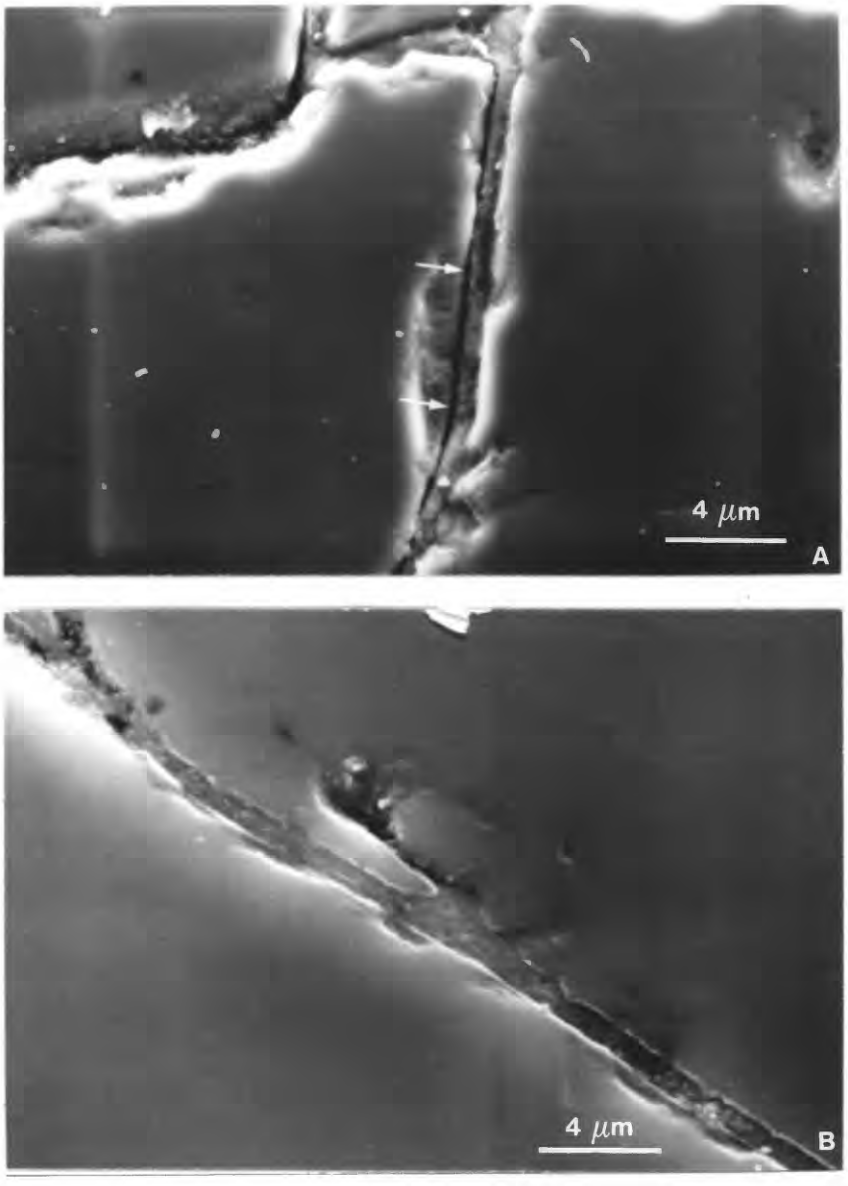

Figure 15.

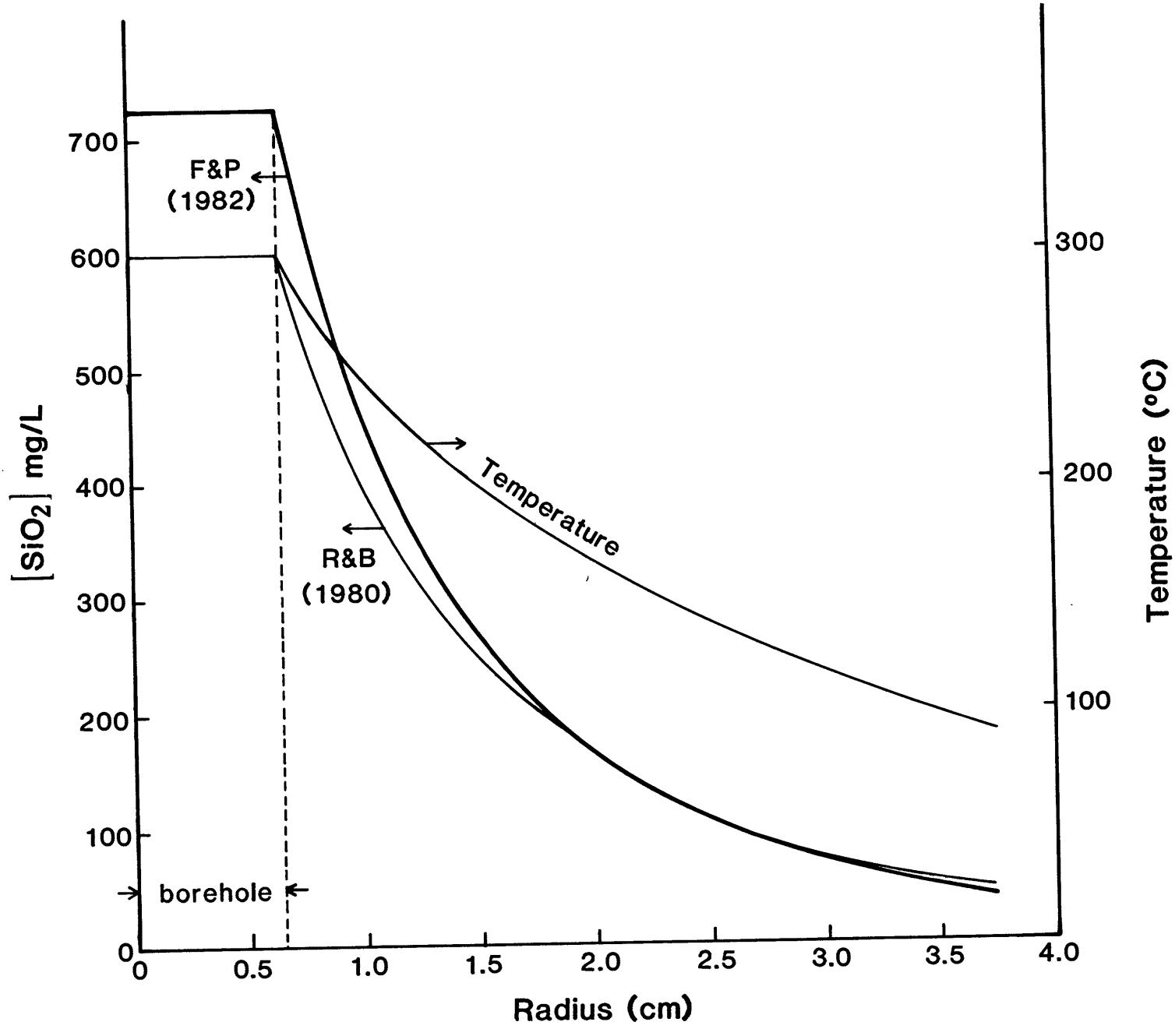
700
600
500
400
300
200
100
0
F&P
(1982)
R&B
(1980)
Temperature
borehole
[SiO2] mg/L
0
0.5
1.0
1.5
2.0
2.5
3.0
3.5
4.0
Radius (cm)
300
200
100
Temperature (°C)

Figure 16.

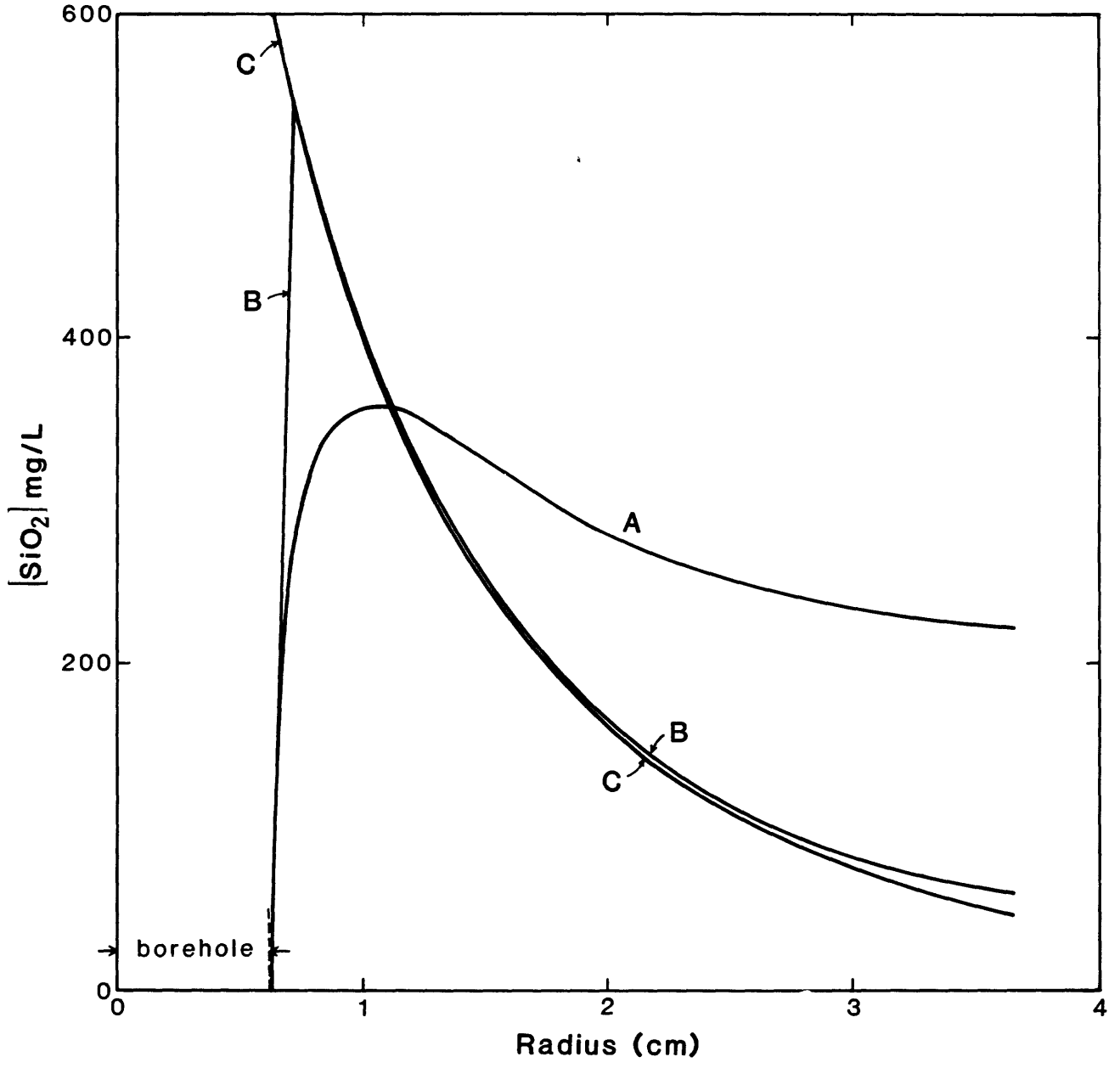

Figure 17.

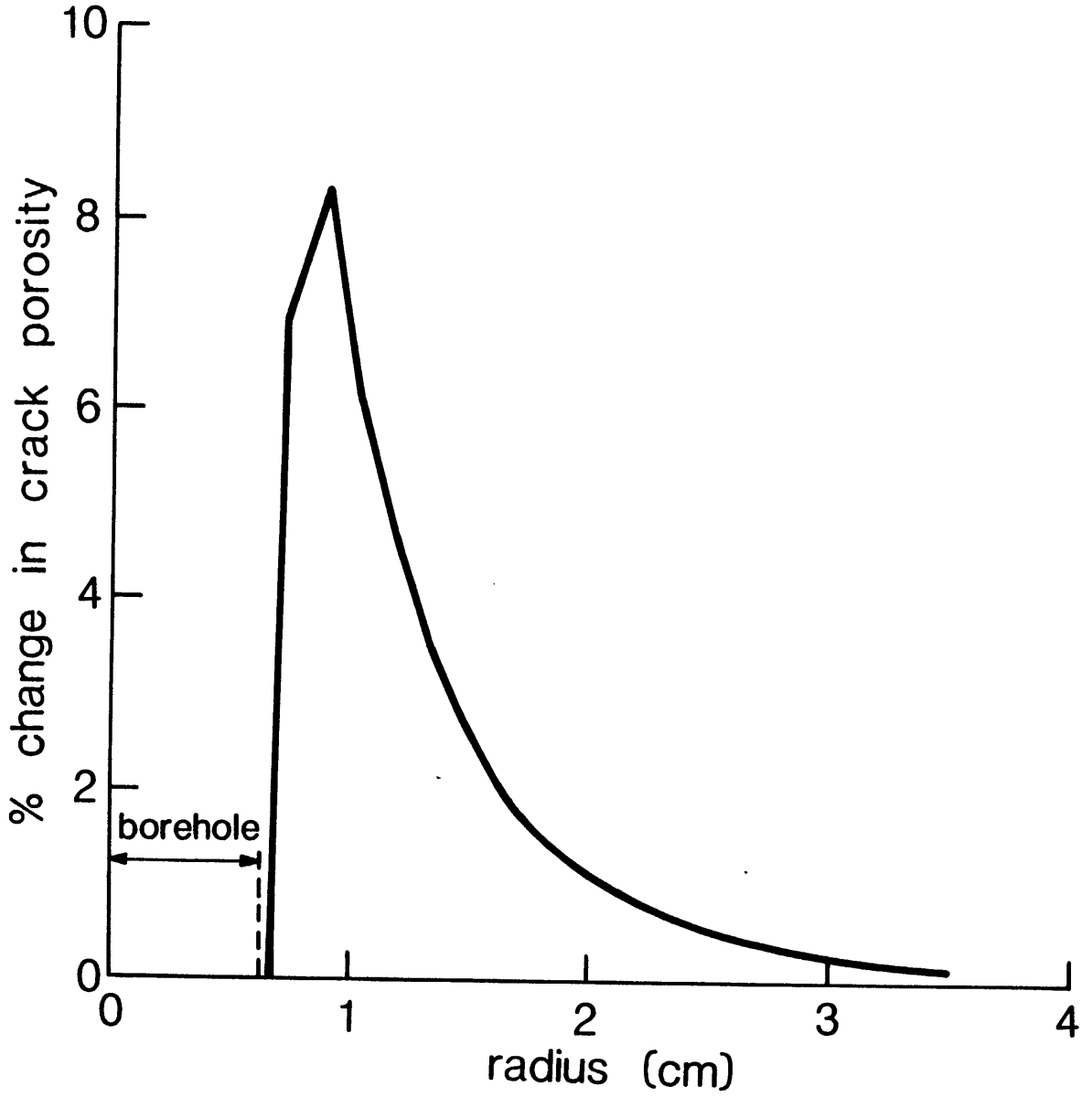

Figure 18.

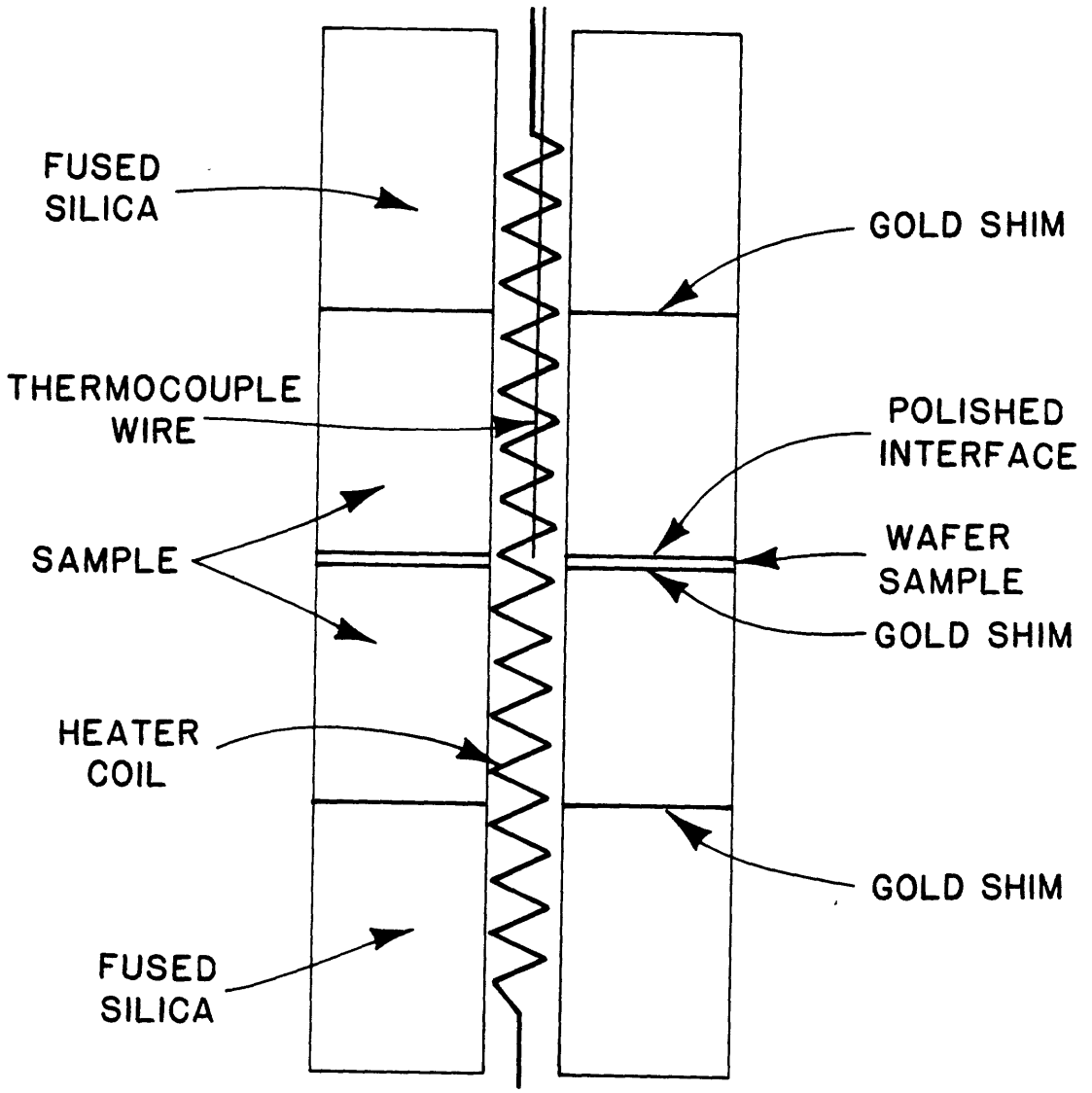
FUSED
SILICA
GOLD SHIM
THERMOCOUPLE
WIRE
POLISHED
INTERFACE
SAMPLE
WAFER
SAMPLE
GOLD SHIM
HEATER
COIL
GOLD SHIM
FUSED
SILICA

Figure 19.

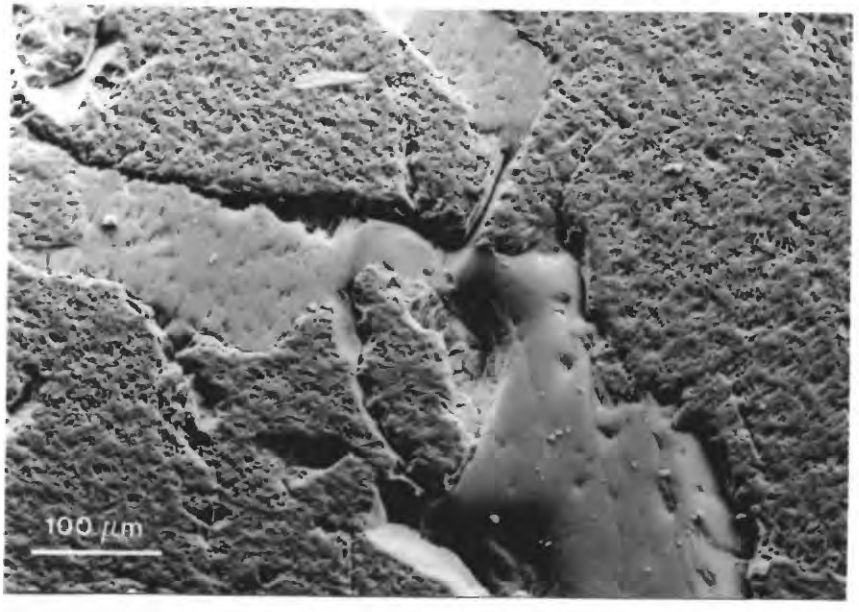

Figure 20.